Cell Reports

Resource

Integrated multi-omics profiling characterizes the crucial role of human dental epithelium during tooth development

Graphical abstract

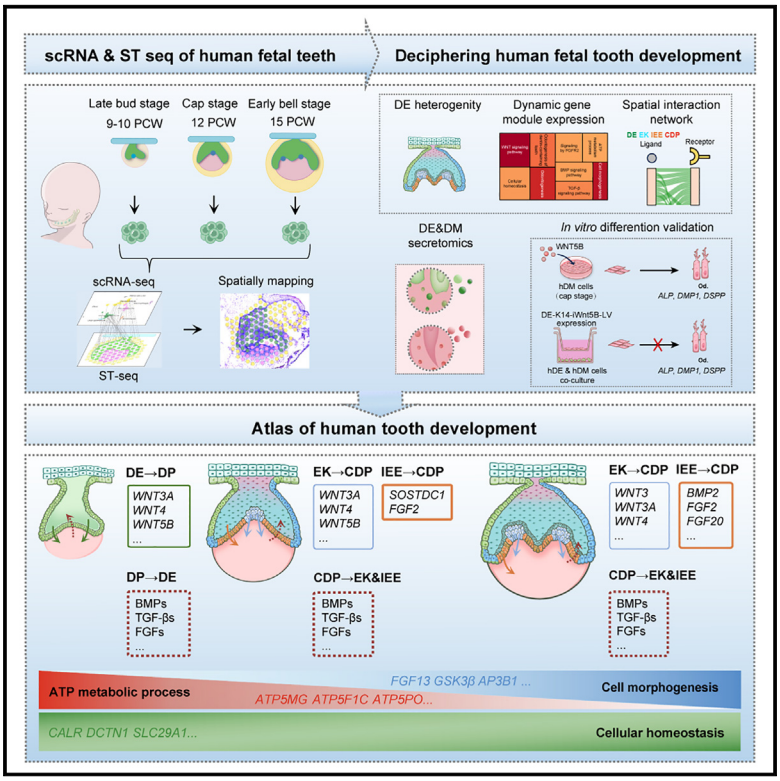

Highlights

- Identified epithelial subpopulations with unique gene expression and spatial patterns
- Discovered epithelium-derived factors facilitating mesenchymal cell development
- Characterized dental epithelium's crucial role in epithelial-mesenchymal interactions
- Developed a public web resource for early human tooth development

Authors

Ran Zhang, Zongshan Shen, Zhenni Zhao, ..., Xiaoshan Wu, Paul T. Sharpe, Songlin Wang

Correspondence

slwang@ccmu.edu.cn

In brief

This study integrates single-cell RNA sequencing, spatial transcriptomics, and secretome analysis to map human fetal tooth development. Zhang et al. uncover dynamic epithelial-mesenchymal interactions, identify crucial signaling factors, and provide a comprehensive resource for future studies on tooth regeneration and related diseases.

Zhang et al., 2025, Cell Reports *44*, 115437
April 22, 2025
https://doi.org/10.1016/j.celrep.2025.115437

CellPress

Cell Reports

CellPress
OPEN ACCESS

Resource

Integrated multi-omics profiling characterizes the crucial role of human dental epithelium during tooth development

Ran Zhang,[1,2] Zongshan Shen,[1,4] Zhenni Zhao,[2] Xiuge Gu,[1] Tianxing Yan,[2] Wei Wei,[1] Chuan Wu,[1] Jinxuan Xia,[1] Yuanyuan Zhang,[8] Suwen Chen,[8] Linsha Ma,[1,5] Dong Zhang,[1,5] Xiaoshan Wu,[1,6] Paul T. Sharpe,[7] and Songlin Wang[1,3,5,6,9,*]

[1]Beijing Laboratory of Oral Health, School of Basic Medical Sciences, Capital Medical University, Beijing, China
[2]Department of Oral Pathology, Peking University School and Hospital of Stomatology & National Center of Stomatology & National Clinical Research Center for Oral Diseases & National Engineering Research Center of Oral Biomaterials and Digital Medical Devices, Beijing, China
[3]Laboratory of Homeostatic Medicine, School of Medicine and SUSTech Homeostatic Medicine Institute, Southern University of Science and Technology, Shenzhen, China
[4]Hospital of Stomatology, Guangdong Provincial Key Laboratory of Stomatology, Guanghua School of Stomatology, Sun Yat-sen University, Guangzhou, China
[5]Immunology Research Center for Oral and Systemic Health, Beijing Friendship Hospital, Capital Medical University, Beijing, China
[6]Academician Workstation for Oral-Maxillofacial Regenerative Medicine, Central South University, Changsha, China
[7]Centre for Craniofacial and Regenerative Biology, King's College London, London SE1 9RT, UK
[8]Beijing Obstetrics and Gynecology Hospital, Capital Medical University/Beijing Maternal and Child Health Care Hospital, Beijing, China
[9]Lead contact
*Correspondence: slwang@ccmu.edu.cn
https://doi.org/10.1016/j.celrep.2025.115437

SUMMARY

The development of early human tooth primordia is not well understood. Here, we linked single-cell RNA sequencing, spatial transcriptomics, and secretome analysis to characterize human fetal tooth development over time. A spatiotemporal atlas of human tooth development at multiple levels was mapped, identifying previously uncharacterized epithelial subpopulations with distinct gene expression profiles and spatial localization. Dynamic changes in epithelial-mesenchymal interactions across developmental stages were characterized. Secretome analysis confirmed the extensive paracrine signaling from the epithelial to mesenchymal compartments and uncovered signaling factors produced by dental epithelium (DE) that regulate mesenchymal cell fate and differentiation. Integration of these datasets highlighted the crucial role of the DE in orchestrating tooth morphogenesis. Our multi-omics approach not only provides unprecedented insights into the cellular and molecular mechanisms of ectoderm-derived tissue development but also serves as a valuable resource, which is publicly available online, for future studies on human tooth regeneration and related diseases.

INTRODUCTION

Teeth, organs essential for chewing food and communication, are the hardest substances in the human body. Mammalian tooth development is a complex process that is orchestrated by a network of signaling molecules and involves intricate interactions between the dental epithelium (DE) and the underlying mesenchyme.[1] Comprehending the molecular mechanisms of tooth development is crucial for fundamental developmental biology, tissue regeneration, as well as for the treatment of dental abnormalities. However, our knowledge of early human tooth development, especially at the cellular and molecular dimensions, remains constrained.

Tooth development progresses through bud, cap, and bell stages, akin to other ectoderm-derived organs.[2] The DE initiates this process by providing instructive signals recognized as a key driver of tooth morphogenesis.[3] Classic tissue recombination experiments have shown that human DE retains odontogenic potential until the bell stage and can induce tooth formation when combined with non-dental mesenchyme.[4] Previous molecular studies have identified various signaling molecules and transcription factors expressed in the DE that play crucial roles in tooth development.[5,6] However, the full extent of epithelial heterogeneity and the specific roles of different epithelial subpopulations in human tooth development remain to be elucidated.

Molecular insights into tooth development have traditionally been derived from genetic mouse models and other animal models, such as miniature pigs[7] and ferrets,[8] with limited consideration for changes in cell populations and tooth types over the 60–100 million years leading to primate evolution. Recent technological advancements have significantly enhanced our capacity to investigate developmental processes with unprecedented

precision. A recent study utilized the single-cell combinatorial indexing RNA sequencing (sci-RNA-seq) technique to identify main cell clusters and signaling pathways in human fetal teeth.[9] However, this study primarily focused on late differentiation stage events, and the sci-RNA-seq technique exhibited constraints in output genes and sensitivity in cell type identification.[10] The integration of single-cell RNA sequencing (scRNA-seq) with spatial transcriptomics (ST) has emerged as a potent approach for delineating gene expression patterns within tissue contexts.[11] These methodologies retain spatial information, enabling researchers to correlate gene expression profiles with specific anatomical locations within the developing tooth. This spatial context is particularly crucial for comprehending the intricate epithelial-mesenchymal interactions (EMIs) steering tooth morphogenesis. Another pivotal facet of tooth development is the DE secretome, encompassing the array of proteins secreted by cells into their extracellular milieu.[12] Secreted factors play indispensable roles in cell-cell communication, tissue patterning, and morphogenesis. Notably, secreted signaling molecules like wingless-type MMTV integration site family (WNTs),[13] bone morphogenetic proteins (BMPs),[14] and fibroblast growth factors (FGFs)[15] have been demonstrated to be indispensable for proper tooth formation. Nevertheless, a comprehensive analysis of the secretome during human tooth development remains unreported in the existing literature.

In this study, 10×Chromium scRNA-seq in conjunction with ST was employed to investigate human fetal tooth development in both spatial and temporal dimensions. Secreted proteins of DE and dental mesenchyme (DM) were mapped, compared, and verified. We revealed previously uncharacterized subpopulations within the DE exhibiting distinct gene expression patterns and spatial distribution. We dynamically characterized EMIs, highlighting the significant role of the DE. Furthermore, epithelial-derived factors were identified and shown to govern mesenchymal cell fate and differentiation. This research represents a significant step forward in our understanding of human tooth development, provides a unique integrated online multi-omics resource for comprehending human development and diseases, and offers insights for formulating and refining hypotheses in tissue regeneration.

RESULTS

Spatially resolved single-cell transcriptomics of developing embryonic human teeth

scRNA-seq profiles were generated from six human tooth samples (one molar and one incisor at each developmental stage) collected from six individuals spanning 9–15 post-conception weeks (PCW), representing three main developmental stages (Figures 1A and S1A). Overall, 65,460 cells with an average expression of 4,597 genes per cell passed quality control (Figure S1B). Uniform manifold approximation and projection (UMAP) dimension reduction analyses depicted clear spatial segregation of spots belonging to specific clusters from human fetal tooth samples (Figure 1B). Unlike the mouse incisors, which grow continuously,[16] human incisors grow similarly to human molars.[9] By merging these two sample types, we discovered that the clusters identified in incisor and molar samples remained consistent throughout the three developmental stages, with all clusters identified in six samples (Figures S1C). Among these, DE, dental papilla (DP), and dental follicle (DF) cells were the top three main cell clusters (Figure 1B).

Differentially expressed gene (DEG) analysis split cells into eight compartments, annotated by transcriptional signatures: DE (*IRX2*$^+$), DP (*RSPO4*$^+$), DF (*FOXF2*$^+$), oral epithelium (OE) (*KRT6B*$^+$), endothelial (*PECAM1*$^+$), macrophage (*IL1B*$^+$), glial (*RAB32*$^+$), and perivascular (*KCNE4*$^+$) (Figures 1C, S1D, and S1E). Bar plots showed DE, DP, and DF cell subcluster proportions based on scRNA-seq (Figure 1D). Gene Ontology (GO) enrichment analyses were conducted on highly expressed genes in the DE, DP, and DF clusters to elucidate the functions of each cell type. In the DE clusters, enrichment of GO terms related to odontogenesis of dentin-containing teeth and cell-cell signaling by WNT suggested a critical role of DE in tooth formation from bud to bell stages, with a likely dependence on WNT signaling. Similarly, GO enrichment in the DP clusters indicated a T cell factor-dependent response to epithelial WNT signaling. Furthermore, enrichment analysis revealed the involvement of Rho GTPase signaling pathway genes and activation of HOX genes during differentiation in the DP cell cluster. The DF cell cluster also exhibited enrichment in WNT-mediated cell-cell signaling and molecules linked to elastic fibers, aligning with the DF's function in periodontium-related structures (Figure 1E).

To further understand the role of DE in human fetal tooth development, cell-cell communication was analyzed using CellChat.[17] The number of incoming and outgoing interactions in each cluster was assessed across different developmental stages (9–10, 12, and 15 PCW), and the total interactions among different cell populations were compared. The edge width is proportional to the number of interactions, which determines how many ligand-receptor pairs contribute to communication between two interacting cell populations. The number of interactions between DE and other groups was consistently high, supporting the crucial role of DE in early tooth development. Comparison of communication probabilities from cell-cell clusters in these signaling pathways revealed DE as the major sender in multiple signaling pathways such as WNT,[5] natriuretic peptide receptor 2 (NPR2),[18] platelet-derived growth factor (PDGF),[19] and parathyroid hormone (PTH)[20] signaling pathways, associated with morphogenesis, odontogenesis, angiogenesis, and homeostasis of calcium and phosphate. Apart from DE, OE cells were also the primary contributors of WNT signaling, while DP and DF cells consistently acted as receivers for WNT signaling throughout the developmental stages. NPR2 signaling originated mainly from DE cells and transiently from perivascular cells at 12 PCW. Endothelial cells were also the primary source of PDGF signaling across all stages. Perivascular cells mainly sent PTH signaling at 9–10 PCW and again at 15 PCW (Figure 1F and S1F-S1I).

To understand the spatial distribution of cells during human tooth development, 10× Visium ST was conducted on teeth (one molar and one incisor) at 9–10, 12, and 15 PCW (1,700 spots, 3,500 genes/spot). Spatial cell clusters focusing on DE, DP, and DF cells were predicted in combination with the scRNA-seq data (Figure 1G and S1J). The spatial expression of marker genes identified in the DE, DP, and DF clusters was

CellPress
OPEN ACCESS

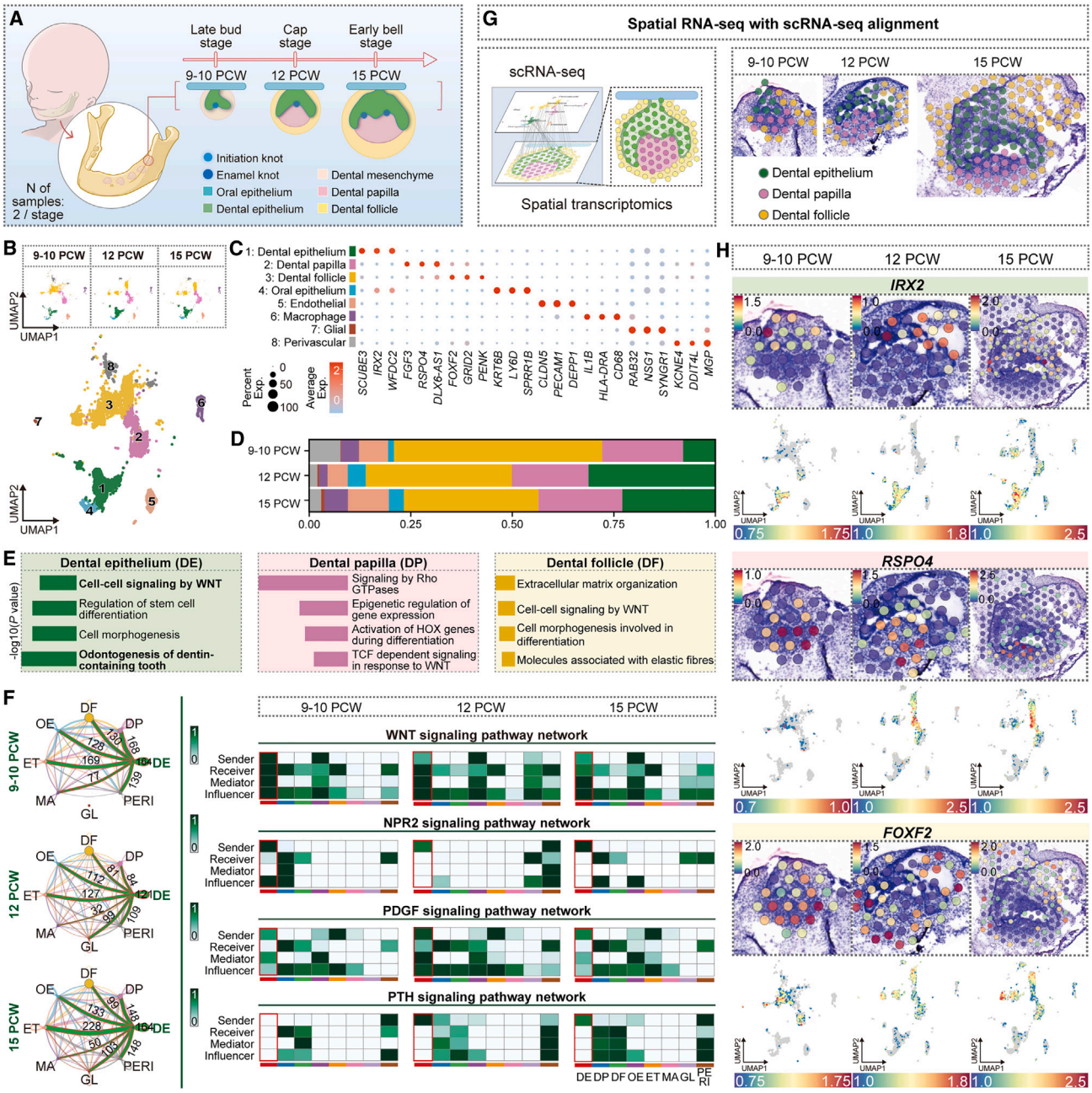

Figure 1. ST combined with scRNA-seq reveals the major cell types of developing human teeth

(A) Overview of the study design for the atlas of human fetal tooth development. PCW, postconceptional week.

(B) UMAP visualization of eight single-cell clusters comprising 65,460 cells was integrated from six scRNA-seq samples.

(C) Markers of tissue-specific genes used for cell annotation shown as a fraction of expressing cells (dot size) and mean expression (color, scaled by *Z* score) of gene markers (rows) across compartments (columns).

(D) Bar plots showing temporal change of cell cluster proportions based on scRNA-seq.

(E) Bar graph showing significantly enriched selected GO terms in DE, DP, and DF clusters.

(F) Circular plots of the cellular interaction numbers revealed by CellChat. The green line indicates high number of interactions in DE clusters. Heatmaps inferring the role of DE as a sender for WNT, NPR2, PDGF, and PTH signaling using CellChat. OE, oral epithelium; ET, endothelial; MA, macrophage; GL, glial; PERI, perivascular.

(G) Alignment of ST spots with scRNA-seq clusters at 9–10, 12, and 15 PCW. All spots were annotated based on scRNA-seq clusters (Figure S1J).

(H) Spatial feature plots of marker genes for DE, DP, and DF subclusters in each sample at 9–10, 12, and 15 PCW.

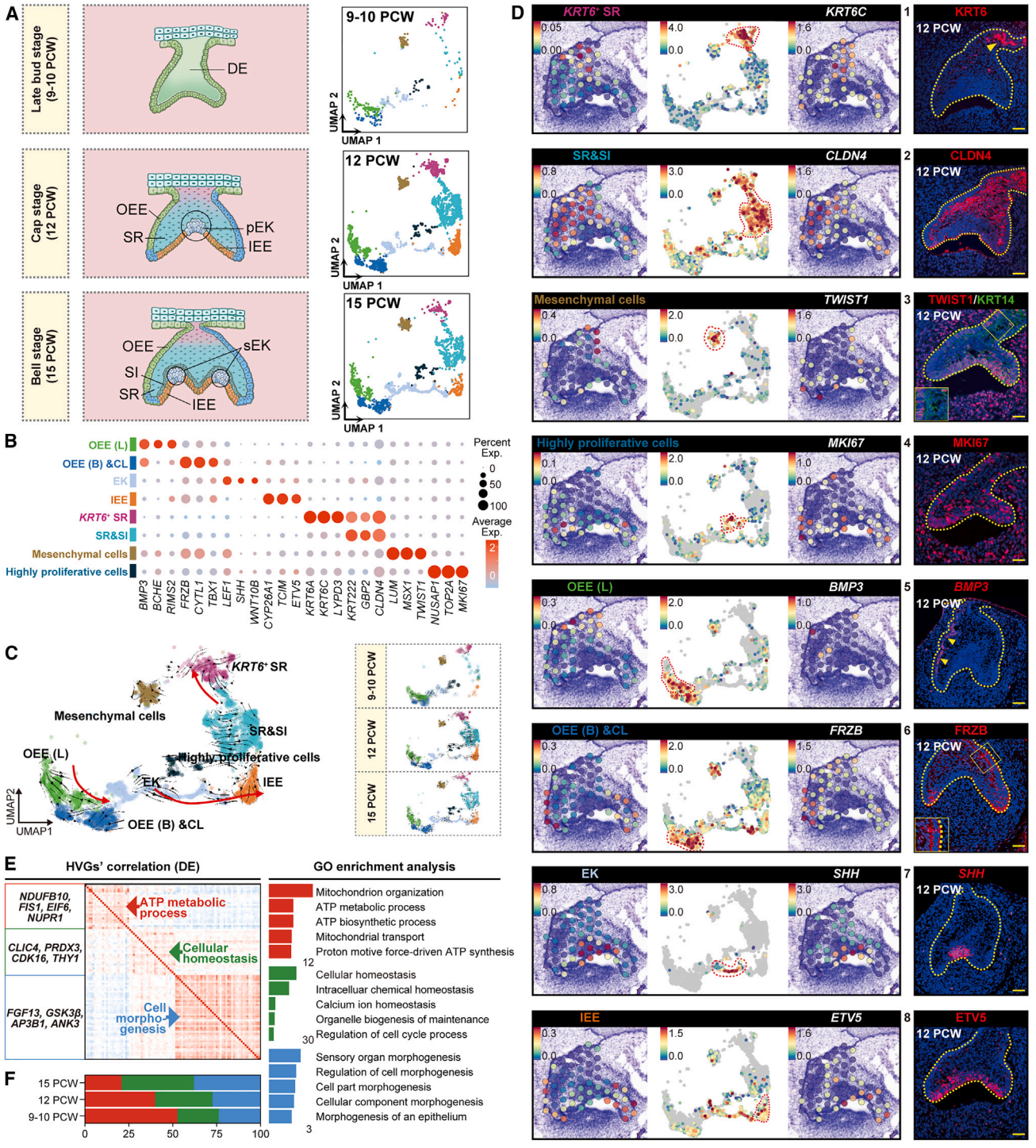

Figure 2. Characterization of human DE cell types in space and time

(A) UMAP projection of scRNA-seq from DE cells clustered by gene expression, colored by cell types. Schematic representation of morphogenic changes in DE through the three developmental stages.

(B) Dot plot of top genes defining subpopulations of DE cells. Cells are colored according to cell clusters.

(C) RNA velocity results on UMAP from scRNA-seq of DE, showing the developmental trajectories of DE. Cells are colored according to cell clusters. Lines indicate the direction of differentiation.

(legend continued on next page)

examined to assess the sensitivity of the method in detecting transcripts per spot. *IRX2* was highly expressed in the DE cluster, while *RSPO4* was mainly expressed in the DP cluster, and *FOXF2* was focally expressed in the DF cluster. Separate UMAP plots for each individual stage were also used to compare them with the corresponding spatial data, showing a dynamic change in gene expression patterns based on scRNA-seq data that correspond well with ST data (Figure 1H).

Human DE exhibits high heterogeneity from late bud to bell stages

During tooth development from the bud to the bell stage, DE sent the highest number of interactions to other clusters. Previous studies have shown that tooth inductive signals can be retained in human DE until the bell stage.[4] Therefore, we focused on DE subtypes and their dynamic gene expression patterns. To achieve this, we integrated the cell atlas of three different stages based on the marker genes listed in the dot plot and feature plots (Figures 2A, 2B, S2B, and S2C). RNA velocity,[21] which can estimate the future states of cells by analyzing spliced and unspliced variants of mRNA in single-cell data to predict the transition potency and directionality of a cell or group of cells, was utilized on the UMAP from the scRNA-seq data of DE to uncover possible fates (Figure 2C). A velocity trend toward the enamel knot (EK) and inner enamel epithelium (IEE) was observed in the lingual outer enamel epithelium (OEE) (Figure 2C), which was further supported by Monocle 3[22] showing a similar trajectory (Figures S2E–S2G). Stellate reticulum (SR) and stratum intermedium (SI) cells were biased toward *KRT6*$^+$ SR cells, which have signatures associated with epidermal development (Figure S3A). This suggests that *KRT6*$^+$ SR cells are likely to be precursors of Serre's glands, which are epithelial remnants of the dental lamina. Some of these cells may proliferate to produce clusters of epithelial cells with tightly packed keratin centrally, a signature seen only in diphyodont animals.[23]

Eight subgroups of DE cells were identified to explain the high heterogeneity within human DE cells based on scRNA-seq, ST, and RNAscope *in situ* hybridization (ISH)/immunofluorescence (IF) staining (Figures 2D and S2D), and GO enrichment analysis was also conducted to show the functions of each cluster (Figure S3A). (1) *KRT6*$^+$ SR cells (*KRT6A*$^+$, *KRT6C*$^+$, *LYPD3*$^+$) were located in the upper area of the SR and connected to the OE. GO enrichment analysis revealed that their functions were related to epidermal development. (2) Compared to *KRT6*$^+$ SR, this cell cluster was found to function in focal adhesion. (3) Epithelial to mesenchymal transition (EMT) is a morphogenetic cell conversion program of epithelial cells to mesenchymal cells and is a key process during embryogenesis and organogenesis.[24] A group of DE cells located adjacent to DM with mesenchymal and EMT markers (*LUM*$^+$, *MSX1*$^+$, *TWIST1*$^+$) was found. Notably, this cell cluster was related to ECM development, ossification, and mesenchymal development according to GO enrichment analysis, suggesting an EMT process during early human tooth development. (4) Highly proliferative cells (*NUSAP1*$^+$, *TOP2A*$^+$, *MKI67*$^+$) were mainly located in the cervical loop (CL) and IEE regions. (5) The lingual portion of OEE cells (*BMP3*$^+$, *BCHE*$^+$, *RIMS2*$^+$) was a distinct cell cluster from the OEE, and its significant function was ossification. (6) GO enrichment of the buccal portion of OEE and the CL cell cluster (*FRZB*$^+$, *CYTL1*$^+$, *TBX1*$^+$) was the WNT signaling pathway. The heterogeneity of OEE cells suggests that they play different roles and have different cell fates during early tooth development. (7) EK cells (*LEF1*$^+$, *SHH*$^+$, *WNT10B*$^+$) were first visible as the initiation knot at 9–10 PCW in the single-cell data, located at the tip of the tooth bud. They then became evident at 12 PCW, called the primary EK (pEK), and at 15 PCW, named the secondary EK (sEK). These cells were located in the center of the tooth bud at 12 PCW in the form of a condensed cell cluster. As a signaling center, the signatures of EK cells were axon development and the WNT signaling pathway, based on GO enrichment analysis. (8) IEE cells (*CYP26A1*$^+$, *TCIM*$^+$, *ETV5*$^+$) appeared at 12 PCW and were precursors of ameloblasts interacting with coronal dental papilla (CDP) cells to form tooth enamel and dentin, respectively. GO enrichment analysis of this cell cluster confirmed its role in ossification. A role for WNT signaling was also observed in this cell cluster.

Dynamic gene expression of three modules including ATP metabolic process, cellular morphogenesis, and cell homeostasis in human DE cells

To gain insight into the transcriptional and molecular mechanisms regulating DE populations, weighted correlation network analysis[25] was utilized to identify co-expressed gene modules and explore core genes. First, the Pearson's correlation coefficients for each pair of genes across all cells were computed. Hierarchical cluster analysis of the correlation matrix revealed three gene modules. Module 1 was enriched in genes related to ATP metabolic processes, such as *NUPR1*, *FIS1*, and *NDUFB10*. Module 2 was enriched with genes such as *THY1*, *CDK16*, and *SLC29A1*; interestingly, genes in this module were associated with cell homeostasis. Module 3 contained genes related to cellular morphogenesis, including *FGF13*, *GSK3*β, and *ANK3* (Figure 2E).

Next, we examined the temporal activity of these three modules and found that the gene expression of module 1 (ATP metabolic process) accounted for 52% of 9–10 PCW samples, followed by a decline in contribution at later stages (40% at 12 PCW and 21% at 15 PCW). These results suggest that ATP metabolic processes serve as a trigger for early tooth development and then turn off their expression, similar to previous reports that transient release of ATP at a certain time could trigger gene expression necessary for eye formation.[26] The genes

(D) Alignment of ST spots with scRNA-seq subclusters in DE (Figure S2D) and comparison of gene expression detection across scRNA-seq, ST, and RNAscope ISH/IF for marker genes specific to each subpopulation on 12 PCW samples (n = 3 technical replicates from five biological replicates). Yellow arrowheads point to the positive signals. Scale bars: 50 μm.

(E) Heatmap showing hierarchical clustering of genes that were most variably expressed by DE cells into three modules, based on gene-gene Pearson's correlation. Representative genes indicated for each gene module. GO (biological process [BP]) enrichment analysis of genes in each module.

(F) Graph showing the relative contributions of cells at various developmental stages to the total gene expression in each module.

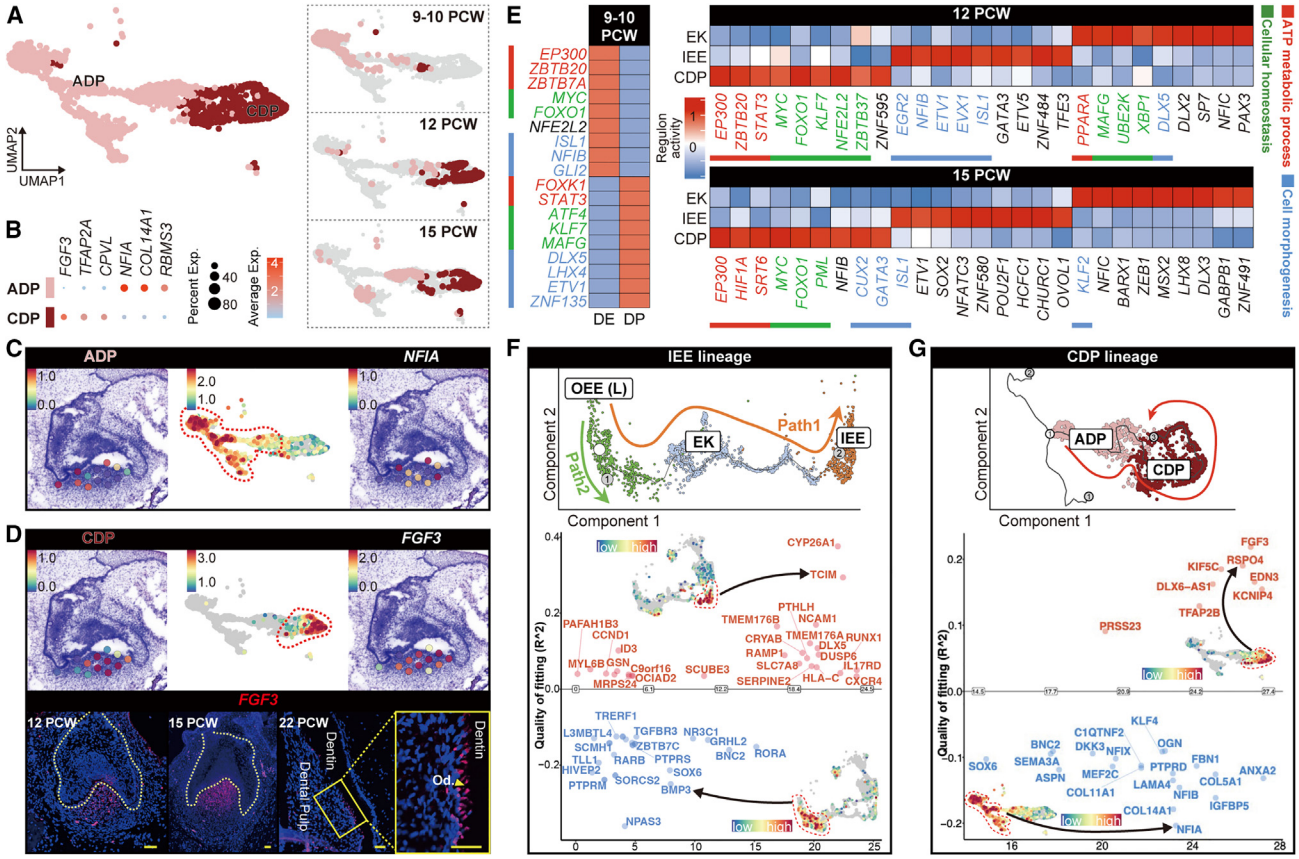

Figure 3. Heterogeneity in DP cells and developmental trajectory with pseudotime

(A) UMAP representation of two color-coded clusters defining regional transcriptome diversity in DP cells.

(B) Dot plot showing the expression level of marker genes for each cluster in different colors.

(C and D) Comparison of gene expression detection across scRNA-seq and ST alignment (Figure S4B), scRNA-seq, and ST for ADP and CDP. RNAscope ISH staining of *FGF3* in human fetal molars at 12, 15, and 22 PCW (n = 3 technical replicates from five biological replicates). Yellow arrowhead indicates positive signals in odontoblasts. Od., odontoblast. Scale bars: 50 μm.

(E) Heatmap of cell-type-specific regulons and selected top enriched regulons in main cell populations at 9–10, 12, and 15 PCW. Representative genes related to each gene module are highlighted by color.

(F and G) GeneSwitches analysis of scRNA-seq data. Linear trajectory inferred by Monocle 2 for the differentiation of OEE (L) to IEE, and ADP to CDP. Visualization of the order of the top switching genes from various sets of known proteins along the pseudotime. The absolute value of the y axis is the quality of fitting defined by McFadden's pseudo-R^2; positive and negative signs indicating up- and down-regulation, respectively.

related to cell homeostasis in module 2 (cellular homeostasis) were expressed consistently, with cells at all developmental stages contributing (24% at 9–10 PCW, 33% at 12 PCW, and 41% at 15 PCW). In module 3 (cell morphogenesis), 24% of the gene expression was associated with 9–10 PCW cells, with a constantly increasing contribution at later developmental stages (27% at 12 PCW and 38% at 15 PCW), suggesting a late morphogenic program (Figure 2F).

Spatial mapping of gene expression profiles in the spatial transcriptomic data further confirmed the dynamic expression patterns of ATP metabolic processes, cellular homeostasis, and cell morphogenesis genes. Notably, the spatial mapping of ATP metabolic-process-related genes revealed focused expression in the IEE region, implying a heightened energy-consuming process during IEE differentiation. Violin plots and spatial feature plots showed the expression of representative genes for each module (Figure S3B). GO analysis was then applied to map the dynamic changes in the functional characteristics of DE from the late bud to bell stages. Consistent with previous findings, most of the significantly enriched GO terms belonged to WNT signaling, odontogenesis, and cell morphogenesis at the three developmental stages. Temporal dynamic changes in GO terms related to ATP metabolic processes and cellular homeostasis were in line with the previous results (Figure S3C).

Cellular heterogeneity of DP and gene regulatory networks of EK, IEE, and CDP in space and time

DP cells were categorized based on their dental pulp and odontoblast lineages, defining two cell clusters through unsupervised clustering and gene signatures. The apical DP (ADP) cell cluster (*NIFA*$^+$, *COL14A1*$^+$, and *RBMS3*$^+$) predominated among DP cells at 9–10 PCW. By 12 PCW, it evolved into two distinct cellular domains, as depicted in Figures 3A and 3B, with the proportion of coronal CDP cell clusters (*FGF3*$^+$, *TFAP2A*$^+$, and *CPVL*$^+$)

beginning to increase. Similar to findings in mice from a previous study,[27] the *FGF3*$^{+}$cell population was considered a precursor of odontoblasts, supported by *FGF3* staining of odontoblasts at 22 PCW, a late bell stage (Figures 3C and 3D). Throughout the late bud to bell stages, EK, IEE, and CDP play pivotal roles in tooth morphogenesis and hard tissue formation. To elucidate the mechanisms governing the lineage development of these three main cell clusters, the single-cell regulatory network inference and clustering (SCENIC)[28] algorithm was employed to predict transcription factors (TFs) with high activity at each developmental direction. Several TF families persistently expressed at the three developmental stages belonged to the aforementioned three gene modules involved in the lineage maintenance of EK, IEE, and CDP. For instance, *EP300*, *ZBTB20*, and *ZBTB7A* belonged to the ATP metabolic process module; *FOXO1*, *MYC*, and *KLF7* were in the cellular homeostasis module; and *ISL1*, *GATA3*, and *DLX5* were in the cellular morphogenesis module (Figure 3E). As IEE and CDP are the two main cell clusters involved in forming tooth hard tissues, GeneSwitches analysis was applied to elucidate their cell fate determination.[29] Several markers identified in this lineage were "on" in the specific lineages (Figures 3F and 3G), providing possible evidence to guide human dental hard tissue formation *in vitro*.

Dynamic EMIs regulate differentiation of DE and DP cells

As ectoderm-derived appendages, tooth development involves a series of programmed, sequential, and reciprocal communications between the epithelium and mesenchyme, resulting in the differentiation of both cell clusters.[30] This is also a hallmark of odontogenesis. To decipher this process more precisely, the focus was placed on three cell clusters: EK, IEE, and CDP. Both EK and IEE had close interactions with CDP, with EK serving as a signaling center and a frontier for inducing differentiation of DP cells.[31] The CellPhoneDB[32] was applied, taking into account spatial cellular colocalization when mapping ligand-receptor pairs (Figure 4A). CellPhoneDB considers the multimeric composition of the majority of ligands and receptors, which are highly relevant for the complex regulation of tooth morphogen-related signaling pathways such as WNT, BMP, transforming growth factor (TGF)-β, SHH, FGF, and retinoic acid (RA) signaling (Figure 4A). WNT ligands were mainly sent out by DE/IEE/EK, while members of BMP, TGF-β, and FGF signaling were mainly sent from the DP. In the cap and early bell stages, with the appearance of EK, the expression of *SHH* became evident. This was thought to be a marker for EK and mutations associated with tooth agenesis.[33] The interaction landscape of human tooth development from the bud to bell stages also showed a crucial role of EK cells in the early developmental stage, sending most of the epithelial signals. Ligands persistently expressed through three developmental stages were highlighted, with most of them being associated with tooth agenesis, such as *WNT10A* and *FGF10* (Figure 4B).[33]

Secreted protein profiling of human DE and DM cells

Most of the epithelia act upon the mesenchyme in a secreted manner. To understand the secreted protein profiles of DE, the cap-stage DE was selected, as it is marked by the growth and expansion of the enamel organ and represents morphogenesis and differentiation. Isolated 12 PCW DE and DM tissues were cultured *in vitro*, and the supernatants were collected. The supernatant was then digested, desalinated, and analyzed using liquid chromatography-mass spectrometry (LC-MS)[34] (Figure 5A). Principal-component analysis was used to analyze the differences between samples and repeatability within the groups. Samples in our groups were clustered close to each other, indicating little difference between samples (Figure 5B). The number of secreted proteins identified in each sample, in DE and DM samples, was represented as a Venn diagram (Figure 5C). Proteins secreted by DE cells overlapped with those secreted by DM cells, but the number was much higher (Figure 5D). GO enrichment was conducted for the significant secreted proteins in DE and DM, consistent with previous findings that DE secretome profiles were associated with odontogenesis, regulation of cell migration, and proliferation. Secretome profiles of DM cells were enriched in BMP signaling and ECM organization (Figure 5E). Furthermore, the number of differentially expressed proteins in the DE secretome was compared to that in the DM secretome. Green represents the number of upregulated differential proteins (n = 698), and pink represents the number of downregulated differential proteins (n = 254), indicating that most secreted proteins from DE cells were upregulated compared to those from DM cells (Figure 5F). GO enrichment analysis of proteins that were upregulated and downregulated in the DE secretome compared to the DM secretome indicated that DE mainly functions through the WNT signaling pathway and positively regulates multiple biological processes, whereas DM is significant for ECM organization and TGF-β/BMP signaling (Figure 5G).

DE-derived WNT5B determines DM odontogenic differentiation

The role of epithelial WNT ligands in initiating odontogenic differentiation of DM has been reported previously[5]; however, it remains unknown which WNTs function in this process. Compared to other WNTs that have been widely studied in tooth development, the function of WNT5B in tooth development remains largely unknown. Differences in total protein were reflected by the volcano map, with the green dot in the upper right corner representing the upregulated differential proteins, and the pink dot in the upper left corner representing the downregulated differential proteins. The top upregulated and downregulated proteins were labeled according to their p values. Expression of WNT5B was upregulated in the DE secretome. Selected DE and DM secreted proteins were represented showing upregulated secreted proteins in DE and DM, respectively (Figure 5H). Violin and ST mappings of WNT5B were visualized (Figure 5I). Main receptors for WNT5B include Frizzled (FZD) receptors (*FZD2*, *FZD4*, *FZD5*, *FZD7*, and *FZD8*) and *ROR1/2* receptors,[35] as identified using scRNA-seq (Figure S5F). Primary cap-stage dental mesenchymal cells were isolated and treated with recombinant WNT5B. Odontoblast differentiation markers such as alkaline phosphatase (*ALP*), dentin matrix protein 1 (*DMP1*), and dentin sialophosphoprotein (*DSPP*) were upregulated after culturing with WNT5B recombinase for 3, 7, and 14 days, implying a stimulatory role of WNT5B in the odontogenic differentiation of human DM cells (Figure 5J). Furthermore, in order to evaluate the impact of epithelial WNT5B on promoting DM

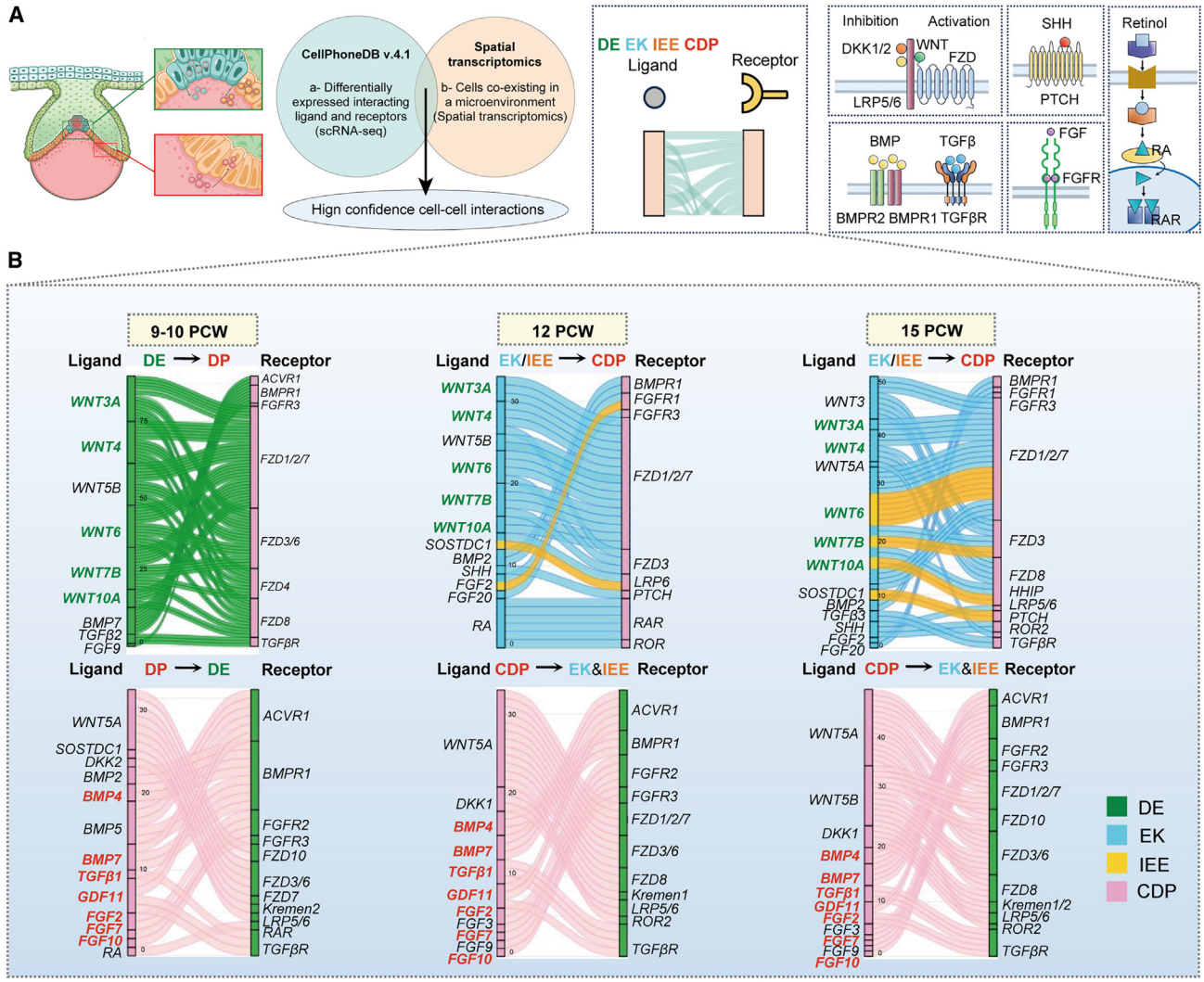

Figure 4. Dynamic signaling interactions between DE and DP modulate critical developmental events in tooth development

(A) Schematic illustration of cell-cell communication tool that considers spatial cellular dynamics between DE and DP. Receptors and ligands involved in critical signaling pathways, WNT, BMP, TGF-β, FGF, and RA signaling.

(B) Alluvial plot showing selected ligand-receptor pairs significantly represented in tooth morphogenesis. For this analysis, only interactions between DE and DP at 9–10 PCW, interactions between EK/IEE and CDP at 12 and 15 PCW, and only ligands and receptors that are differentially expressed ($p < 0.05$) are considered. Genes persistently expressed across the three developmental stages are highlighted by green and red color, respectively.

differentiation and eliminate the cell-autonomous effects of WNT5B in DM differentiation, we developed a keratin 14 promoter-EGFP-miR155-shRNA-WNT5B construct for knocking down *WNT5B* in the co-cultured DE and DM system. Knockdown of *WNT5B* expression from DE cells induced a significant decrease in *WNT5B* expression in DE cells and DE supernatants and a decline in the expression of odontogenic markers in DM cells (Figure 5K). In order to further validate the odontogenic differentiation potential of WNT5B and investigate its potential clinical application in dentin regeneration, WNT5A was utilized as a positive control.[36,37] After 7 days of induction, the expression of odontogenic markers, along with ALP and Alizarin Red S staining, revealed that WNT5B had a more significant stimulatory role than WNT5A. Even a low dose of WNT5B showed a better odontogenic induction effect (Figure 5L). To further demonstrate the pivotal role of DE in early human tooth development, we separated human cap-stage DE and combined it with lip mesenchyme, which harbored no odontogenic signals. The recombinants were then embedded under kidney capsules for 3 months, and they grew into tooth germs with well-differentiated cells with *SHH* expression, an odontogenic marker, as shown in the inset (Figure 5M).

Schematic illustration of a proposed model for spatiotemporal gene expression patterns in human tooth development

A schematic model is proposed to elucidate the significant role of DE in various biological processes during human fetal tooth development, particularly from the late bud to bell stage. The

CellPress
OPEN ACCESS

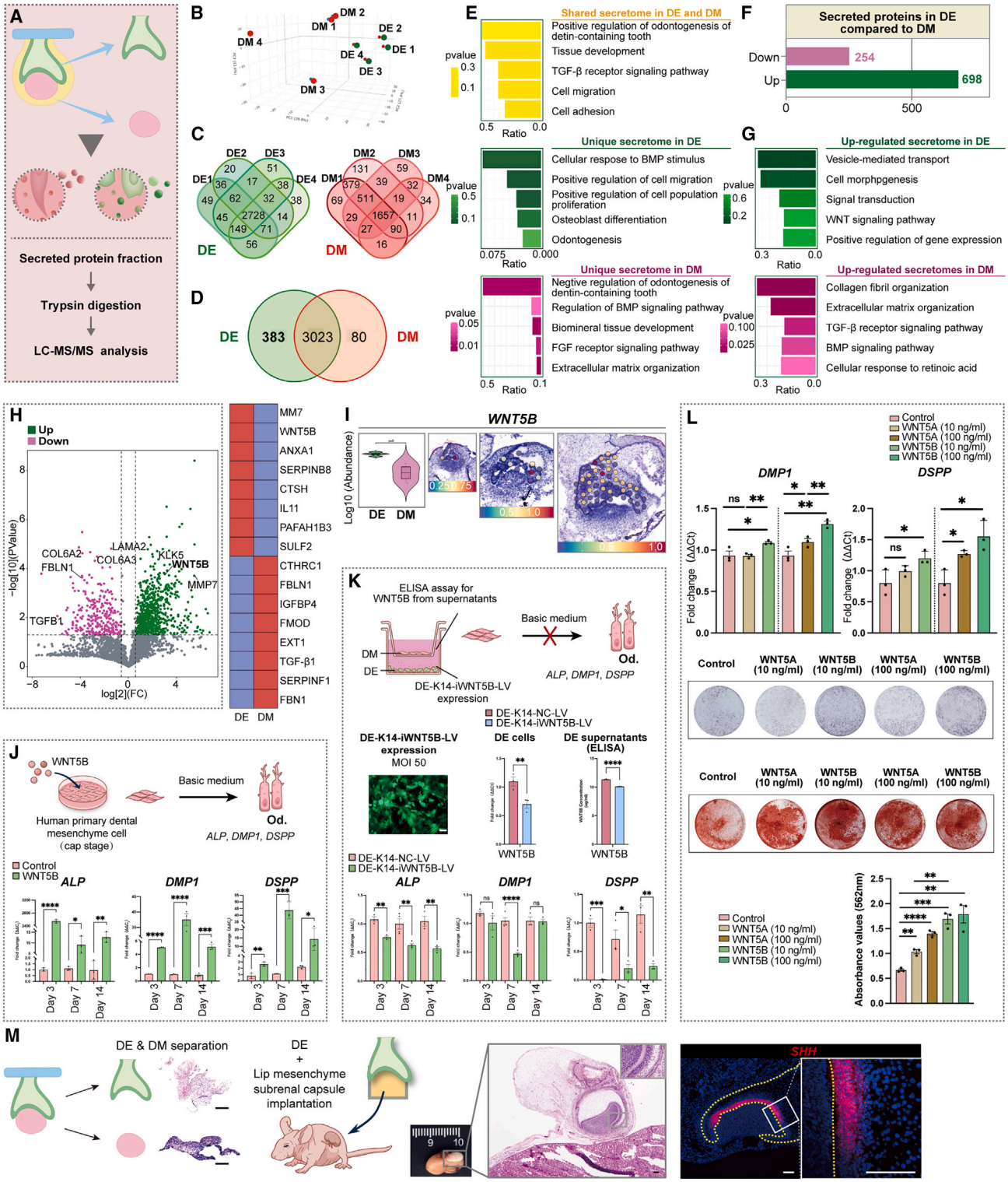

Figure 5. Profiling of human DE and DM secretome by mass spectrometry reveals the critical role of WNT5B regulates DM odontogenic differentiation

(A) Workflow for the analysis of secreted proteins and processed peptides from conditioned medium in DE and DM cells, respectively.

(B) Principal-component analysis (PCA) map visually analyzing the repeatability within DE and DM groups.

(legend continued on next page)

DE consists of eight distinct subpopulations characterized by specific markers. Additionally, DP is categorized into two subpopulations based on their respective location and function. DE cells predominantly transmit morphogenic signals, primarily WNT signals, while DP functions mainly through BMP, TGF-β, and FGF signaling pathways. This signaling pattern is supported by secretome analysis. Notably, epithelial signals originate mainly from the EK rather than the IEE from the cap to bell stage. Furthermore, three gene modules exhibit dynamic expression patterns during the late bud, cap, and bell stages. The expression levels of genes related to ATP metabolism gradually decrease concomitant with the upregulation of cell morphogenic genes. Conversely, the expression of genes associated with cellular homeostasis remains relatively stable and balanced (Figure 6).

DISCUSSION

In this study, we have constructed a comprehensive single-cell transcriptomic atlas that delineates human tooth development from the late bud to the bell stages. Through the integration of scRNA-seq, ST data, and secretome analysis, we have spatially mapped different cell types and elucidated EMI patterns in orchestrating odontogenesis. Epithelial-derived factors have been identified, and the odontogenic role of WNT5B has been characterized. Overall, our findings underscore the crucial role of the DE in regulating multiple early biological processes. Furthermore, the spatiotemporal molecular and cellular atlas of human tooth development data provides valuable online resources for investigating human tooth development and designing regeneration strategies in humans.

Our study presents the characterization of human tooth cell types based on genes associated with specific cell-signaling networks and spatial localization. Significant regulators identified by GO enrichment include WNT signaling, Rho GTPases, and HOX genes based on the analysis. WNT signaling plays a crucial role in cell fate determination, proliferation, and differentiation, particularly in regulating DE, DP, and DF cell clusters during dental development.[38–41] While the function of Rho GTPases in dental papilla development remains largely unexplored, their enrichment in GO terms has attracted attention for their involvement in tooth development, potentially influencing cell shape changes and movement. HOX gene expression in cells derived from cranial neural crest such as DP cells is unexpected but recent studies have demonstrated HOX genes are involved in the regulation of dental stem cell fate and differentiation,[42] and questions persist regarding mechanisms by which HOX genes control dental stem cell decisions, the role of specific HOX genes in different stages of tooth development, and the therapeutic applications of manipulating HOX gene expression in dental regeneration.

The spatial delineation of subsets of human DE cells has been finely detailed. Among the eight epithelial subclusters identified, *KRT6A*$^{+}$ SR was distinguished as a unique signature in diphyodonts, potentially representing the precursor of Serres' glands,[43] a feature commonly found in humans but rare in mice. While recent studies have contributed valuable insights into mouse fetal tooth development, disparities exist between human and mouse dentitions, cell compositions, and gene expression patterns.[16,27,44] In the previous human fetal tooth sci-RNA-seq dataset, the emphasis was on late developmental stages, with early developmental events and cell types being less investigated. Moreover, sci-RNA-seq has limitations in defining a comprehensive range of cell types, which may contribute to discrepancies in cell-type-specific markers between our study and theirs.[9,10] In contrast, our research specifically examined DE from bud to early bell stages. We verified spatial information of DE and DM subclusters by integrating scRNA-seq, ST, and RNAscope ISH to conquer the insufficient resolution of 10× spatial technology that prevents achieving single-cell resolution.[45] Through the comparison of interactions and recombination experiments, our study demonstrated the prominent role of human DE during early human fetal development, aligning with the consensus that DE provides initial tooth inductive signals until the bell stage in humans.[4] Notably, human DE retains its inductive capacity for a longer duration compared to mice, necessitating the preservation of tooth-forming potential in the dental lamina until the bell stage, a critical period coinciding with the emergence of the dental lamina for permanent teeth in humans. Finally, DE cells are lost during tooth eruption, contributing to a scarcity of knowledge compared to DM.[27] While studies have demonstrated the applicability of various epithelial cell sources in whole-tooth bioengineering,[46] our findings offer valuable insights for tooth regeneration strategies by identifying

(C and D) Venn diagrams showing the number of secreted proteins within four independent samples and significant secreted proteins between DE and DM groups.
(E) GO enrichment analysis (BP) of shared secreted proteins and unique secreted proteins in DE and DM cells.
(F) Bar graph representing a significant upregulated number of secreted proteins in DE compared to DM.
(G) GO enrichment analysis (BP) of upregulated proteins in DE and DM cells, respectively.
(H) Volcano plot showing upregulated and downregulated secretome of DE in comparison with DM cells. Heatmap showing the expression of significant secreted proteins in the DE and DM, respectively.
(I) Violin plot showing expression of *WNT5B* in DE and its spatiotemporal mapping.
(J) The stimulatory effect of WNT5B on odontogenic differentiation of human primary DM cells *in vitro* with elevated expression of odontoblast-specific markers. Data are represented as mean ± SEM. *$p < 0.05$, **$p < 0.01$, ***$p < 0.001$, and ****$p < 0.0001$ by Student's t test.
(K) Knockdown of *WNT5B* in DE inhibiting odontogenic differentiation potential of DM cells in a co-culture model. Data are represented as mean ± SEM. *$p < 0.05$, **$p < 0.01$, ***$p < 0.001$, and ****$p < 0.0001$ by Student's t test. Scale bar: 100 μm.
(L) The stimulatory effect of WNT5B on differentiation of human primary DM cells was greater than that of WNT5A. Data are represented as mean ± SEM. *$p < 0.05$, **$p < 0.01$, ***$p < 0.001$, and ****$p < 0.0001$ by Student's t test.
(M) Isolation and combination of cap-stage DE with lip mesenchyme generating a tooth germ under kidney for 3 months with *SHH* expression by RNAscope ISH ($n = 3$ technical replicates from five biological replicates). Scale bars: 50 μm.

CellPress
OPEN ACCESS

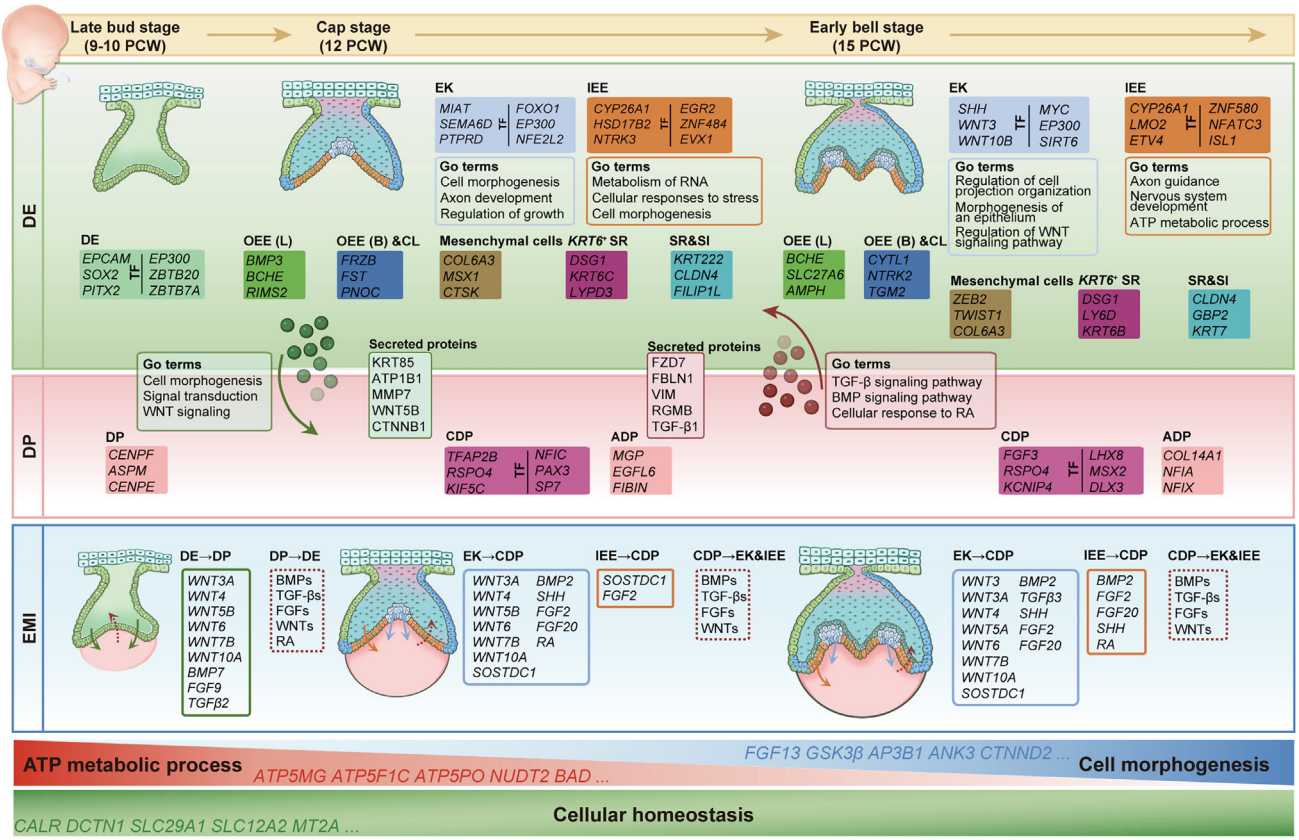

Figure 6. Schematic illustration of human fetal tooth development through space and time

Color-coded schematic drawings of DE and DP subpopulations are shown, with dynamic expression of DEGs highlighted by cell populations from late bud to bell stages. Selected secreted proteins and upregulated secreted proteins in DE and DM at cap stage are presented, along with relevant GO terms. An interaction landscape of DE/EK/IEE and DP/CDP through late bud to bell stages is depicted, showing the dynamic change of three gene-module expressions in DE.

reliable sources of DE cells or stimulating dental epithelial signals for potential clinical applications.

Temporal dynamics of gene modulation during human fetal tooth development were unveiled. The concept of homeostasis,[47] which denotes the dynamic equilibrium maintained by organisms to ensure internal stability and adaptability to external conditions for survival, was exemplified by the balanced expression of homeostasis-related genes across the three developmental stages. A gene module associated with cellular morphogenesis, encompassing genes influencing organismal shape,[48,49] exhibited heightened expression as tooth morphogenesis progressed. The significance of ATP signaling molecules in various developmental processes, particularly in hard tissue formation, was underscored by the increased expression of ATP-related genes in the IEE, suggesting heightened energy requirements for IEE proliferation and differentiation.[50] While the precise functions of genes within these modules necessitate further validation, the observed gene expression patterns in the DE are pivotal for orchestrating tooth development and regeneration.

The EMI atlas of human fetal tooth development was revealed in this study. Key signaling pathways including WNT, BMP, TGF-β, FGF, and SHH were found to guide early tooth development. The atlas, created through scRNA-seq data and spatial information, revealed that WNT signaling predominantly operates in the DE, while BMP, TGF-β, and FGF signaling are more active in the DM. Several genes linked to tooth agenesis, such as *WNT10A*, *FGF3*, *FGF10*, *FGFR3*, *SHH*, and *PTCH1*, were identified,[33,51,52] underscoring the clinical significance of developmental cell atlas initiatives. Consistent with prior research, RA signaling was observed to enhance osteo/odontogenic differentiation of dental pulp stem cells, likely due to epithelial RA secretion.[53] Initially, EK cells in the DE exhibited higher signaling activity compared to adjacent IEE cell clusters, aligning with their role as a signaling center.[54] This depiction of the dynamic interaction landscape enhances our comprehension of tooth development and other ectoderm-derived organogenesis.

This study presents the secreted protein profiles of DE and DM cells. A majority of secreted proteins from DE cells exhibited upregulation compared to those from DM cells, thereby confirming the hypothesized EMI pattern. The expression level of WNT5B was higher in the DE secretome, which corresponds well with the data in the EMI. DE-derived WNT5B interacts with FZD receptors from late bud to cap stage. The role of WNT5B in tooth development is not well understood. This study observed the stimulatory effects of epithelial WNT5B on odontogenic

differentiation in human primary dental mesenchymal cells. Recent research indicates that DE function primarily involves the secretion and absorption of molecules for active transport, underscoring the significance of secreted factors released by DE cells in early odontogenesis.[5,6] The presence of epithelial WNT5B, in conjunction with other protein molecules identified in the DE and DM secretome profiles, contributes to unraveling the implicit messages conveyed by bioactive molecules, the ECM, and other growth factors in the context of tooth development and regeneration. However, further identification of low-abundance factors is needed in future studies.

The integration of scRNA-seq with ST and secretome analysis in this study has revealed a comprehensive atlas of cellular heterogeneity, molecular gene networks, and secreted proteins during human fetal tooth development. These findings offer valuable insights into the underlying mechanisms that may extend to the development of other ectoderm-derived tissues. Moreover, they hold promise for advancements in human tooth regeneration and the elucidation of associated pathologies.

Limitations of the study

We have provided valuable insights into human fetal tooth development, but there are limitations to consider. The ST used has limited resolution and may miss small or rare cell populations, impacting the understanding of cell types involved in tooth development. Our study focuses on early stages of tooth development, from bud to bell stages, but does not cover late stages, leaving a gap in understanding the full developmental trajectory. Secretome analysis, which examines secreted signaling molecules, faces challenges due to the transient and low-abundance nature of these proteins. These limitations underscore the need for further studies, addressing these gaps with advanced technologies and comprehensive analyses to deepen the understanding of tooth morphogenesis and its potential in regenerative medicine.

RESOURCE AVAILABILITY

Lead contact

Please direct any requests for additional information, resources, and reagents to the lead contact, Songlin Wang (slwang@ccmu.edu.cn).

Materials availability

Requests for materials generated in this study should be directed to the lead contact. A completed materials transfer agreement will be required.

Data and code availability

- The scRNA-seq data that support the findings of this study have been deposited into CNGB Sequence Archive (CNSA) of China National GeneBank DataBase (CNGBdb): CNP0006291.
- The ST data have been deposited into StomicsDB database: STT0000140.
- The secretome data generated from this study have been deposited in the OMIX, China National Center for Bioinformation/Beijing Institute of Genomics, Chinese Academy of Sciences: OMIX009173.
- Other data generated from this study are available upon request.
- All code utilized in this study has been previously published, and the pipelines are detailed in the STAR Methods.
- Any further details needed to reanalyze the data presented in this paper can be obtained from the lead contact upon request.

ACKNOWLEDGMENTS

We thank members of Beijing Laboratory of Oral Health for inspiring discussions. We are grateful to Prof. Paul Sharpe for his valuable guidance. We acknowledge Xiangyuan Bai and Guangqiang Yu for their technical support. We appreciate Jingjing Bai, Yuanyuan Zhang, and Jun Wang for sample collection.

AUTHOR CONTRIBUTIONS

Conceptualization, S.W., R.Z., and D.Z.; collection and analysis of scRNA-seq data, R.Z., Z.S., and J.X.; collection and analysis of images and ST data, R.Z. and Z.S.; methodology, Z.Z., X.G., Y.Z., C.W., T.Y., S.C., W.W., P.T.S., and L.M.; funding acquisition, S.W. and R.Z.; writing – original draft, S.W. and R.Z.; writing – review & editing, S.W., R.Z., P.T.S., D.Z., X.W., Z.S., and Z.Z.

DECLARATION OF INTERESTS

The authors declare no conflicts of interest.

STAR★METHODS

Detailed methods are provided in the online version of this paper and include the following:

- KEY RESOURCES TABLE
- EXPERIMENTAL MODEL AND STUDY PARTICIPANT DETAILS
  - Human fetal tooth tissue
  - Establishment of human primary DE and DM cells
- METHOD DETAILS
  - Droplet based scRNA-seq
  - Spatial transcriptomics
  - Primary analysis of raw read data
  - Quality control, dimension reduction and clustering
  - Differentially expressed genes analysis
  - Cell type annotation
  - Subcluster analysis
  - Trajectory analysis
  - GeneSwitches analysis
  - Velocity analysis
  - Gene regulatory network inference
  - Cellular interaction analysis
  - Process and quality control of spatial RNA-seq
  - The identification and quantitation of protein
  - The functional analysis of protein
  - I, RNAscope *in situ* hybridization (ISH) and H&E staining
  - Collection of the supernatant, protein extraction, digestion and desalination
  - Liquid chromatography (LC)-mass spectrometer (MS)/MS analysis
  - Plasmid construction and lentivirus production
  - *In vitro* treatment assay
  - ALP staining
  - Alizarin red S staining
  - RT-qPCR
  - ELISA
  - Tissue recombination and subrenal culture
- QUANTIFICATION AND STATISTICAL ANALYSIS

SUPPLEMENTAL INFORMATION

Supplemental information can be found online at https://doi.org/10.1016/j.celrep.2025.115437.

Received: November 18, 2024
Revised: January 17, 2025
Accepted: February 25, 2025

REFERENCES

1. Pispa, J., and Thesleff, I. (2003). Mechanisms of ectodermal organogenesis. Dev. Biol. *262*, 195–205.
2. Cazares, O., Haque, A.S., and Klein, O.D. (2021). Salivary gland: A budding genius. Dev. Cell *56*, 2271–2272.
3. Modino, S.A.C., and Sharpe, P.T. (2005). Tissue engineering of teeth using adult stem cells. Arch. Oral Biol. *50*, 255–258.
4. Hu, X., Lin, C., Shen, B., Ruan, N., Guan, Z., Chen, Y., and Zhang, Y. (2014). Conserved odontogenic potential in embryonic dental tissues. J. Dent. Res. *93*, 490–495.
5. Xiong, Y., Fang, Y., Qian, Y., Liu, Y., Yang, X., Huang, H., Huang, H., Li, Y., Zhang, X., Zhang, Z., et al. (2019). Wnt Production in Dental Epithelium Is Crucial for Tooth Differentiation. J. Dent. Res. *98*, 580–588.
6. Wang, J., Lin, X., Shen, Z., Li, G., Hu, L., Li, Q., Li, Y., Wang, J., Zhang, C., Wang, S., and Wu, X. (2023). AKT from dental epithelium to papilla promotes odontoblast differentiation. Differentiation *134*, 52–60.
7. Wu, X., Hu, J., Li, G., Li, Y., Li, Y., Zhang, J., Wang, F., Li, A., Hu, L., Fan, Z., et al. (2020). Biomechanical stress regulates mammalian tooth replacement via the integrin beta1-RUNX2-Wnt pathway. EMBO J. *39*, e102374.
8. Jussila, M., Crespo Yanez, X., and Thesleff, I. (2014). Initiation of teeth from the dental lamina in the ferret. Differentiation *87*, 32–43.
9. Alghadeer, A., Hanson-Drury, S., Patni, A.P., Ehnes, D.D., Zhao, Y.T., Li, Z., Phal, A., Vincent, T., Lim, Y.C., O'Day, D., et al. (2023). Single-cell census of human tooth development enables generation of human enamel. Dev. Cell *58*, 2163–2180.
10. Ding, J., Adiconis, X., Simmons, S.K., Kowalczyk, M.S., Hession, C.C., Marjanovic, N.D., Hughes, T.K., Wadsworth, M.H., Burks, T., Nguyen, L.T., et al. (2020). Systematic comparison of single-cell and single-nucleus RNA-sequencing methods. Nat. Biotechnol. *38*, 737–746.
11. Rao, A., Barkley, D., França, G.S., and Yanai, I. (2021). Exploring tissue architecture using spatial transcriptomics. Nature *596*, 211–220.
12. Wei, W., Riley, N.M., Lyu, X., Shen, X., Guo, J., Raun, S.H., Zhao, M., Moya-Garzon, M.D., Basu, H., Sheng-Hwa Tung, A., et al. (2023). Organism-wide, cell-type-specific secretome mapping of exercise training in mice. Cell Metab. *35*, 1261–1279.
13. Lee, J.M., Qin, C., Chai, O.H., Lan, Y., Jiang, R., and Kwon, H.J.E. (2022). MSX1 Drives Tooth Morphogenesis Through Controlling Wnt Signaling Activity. J. Dent. Res. *101*, 832–839.
14. Vainio, S., Karavanova, I., Jowett, A., and Thesleff, I. (1993). Identification of BMP-4 as a signal mediating secondary induction between epithelial and mesenchymal tissues during early tooth development. Cell *75*, 45–58.
15. Li, L., Tang, Q., Kwon, H.J.E., Wu, Z., Kim, E.J., and Jung, H.S. (2018). An Explanation for How FGFs Predict Species-Specific Tooth Cusp Patterns. J. Dent. Res. *97*, 828–834.
16. Krivanek, J., Soldatov, R.A., Kastriti, M.E., Chontorotzea, T., Herdina, A.N., Petersen, J., Szarowska, B., Landova, M., Matejova, V.K., Holla, L.I., et al. (2020). Dental cell type atlas reveals stem and differentiated cell types in mouse and human teeth. Nat. Commun. *11*, 4816.
17. Jin, S., Guerrero-Juarez, C.F., Zhang, L., Chang, I., Ramos, R., Kuan, C.H., Myung, P., Plikus, M.V., and Nie, Q. (2021). Inference and analysis of cell-cell communication using CellChat. Nat. Commun. *12*, 1088.
18. Zhao, Y., Yang, F., Wang, L., and Che, H. (2020). Familial hypophosphatemic rickets caused by a PHEX gene mutation accompanied by a NPR2 missense mutation. J. Pediatr. Endocrinol. Metab. *33*, 305–311.
19. Chai, Y., Bringas, P., Jr., Mogharei, A., Shuler, C.F., and Slavkin, H.C. (1998). PDGF-A and PDGFR-alpha regulate tooth formation via autocrine mechanism during mandibular morphogenesis in vitro. Dev. Dyn. *213*, 500–511.
20. Li, T., Wang, H., Jiang, Y., Chen, S., Huang, D., Wu, Z., Yin, X., Zhou, C., Li, Y., and Zou, S. (2023). LITTIP/Lgr6/HnRNPK complex regulates cementogenesis via Wnt signaling. Int. J. Oral Sci. *15*, 33.
21. La Manno, G., Soldatov, R., Zeisel, A., Braun, E., Hochgerner, H., Petukhov, V., Lidschreiber, K., Kastriti, M.E., Lönnerberg, P., Furlan, A., et al. (2018). RNA velocity of single cells. Nature *560*, 494–498.
22. Cao, J., Spielmann, M., Qiu, X., Huang, X., Ibrahim, D.M., Hill, A.J., Zhang, F., Mundlos, S., Christiansen, L., Steemers, F.J., et al. (2019). The single-cell transcriptional landscape of mammalian organogenesis. Nature *566*, 496–502.
23. Nel, S., Van Heerden, M.B., Steenkamp, G., Van Heerden, W.F.P., and Boy, S.C. (2011). Immunohistochemical profile of odontogenic epithelium in developing dog teeth (Canis familiaris). Vet. Pathol. *48*, 276–282.
24. Thiery, J.P., Acloque, H., Huang, R.Y.J., and Nieto, M.A. (2009). Epithelial-mesenchymal transitions in development and disease. Cell *139*, 871–890.
25. Langfelder, P., and Horvath, S. (2008). WGCNA: an R package for weighted correlation network analysis. BMC Bioinf. *9*, 559.
26. Masse, K., Bhamra, S., Eason, R., Dale, N., and Jones, E.A. (2007). Purine-mediated signalling triggers eye development. Nature *449*, 1058–1062.
27. Jing, J., Feng, J., Yuan, Y., Guo, T., Lei, J., Pei, F., Ho, T.V., and Chai, Y. (2022). Spatiotemporal single-cell regulatory atlas reveals neural crest lineage diversification and cellular function during tooth morphogenesis. Nat. Commun. *13*, 4803.
28. Aibar, S., González-Blas, C.B., Moerman, T., Huynh-Thu, V.A., Imrichova, H., Hulselmans, G., Rambow, F., Marine, J.C., Geurts, P., Aerts, J., et al. (2017). SCENIC: single-cell regulatory network inference and clustering. Nat. Methods *14*, 1083–1086.
29. Cao, E.Y., Ouyang, J.F., and Rackham, O.J.L. (2020). GeneSwitches: ordering gene expression and functional events in single-cell experiments. Bioinformatics *36*, 3273–3275.
30. Yu, T., and Klein, O.D. (2020). Molecular and cellular mechanisms of tooth development, homeostasis and repair. Development *147*, dev184754.
31. Thesleff, I., Keränen, S., and Jernvall, J. (2001). Enamel knots as signaling centers linking tooth morphogenesis and odontoblast differentiation. Adv. Dent. Res. *15*, 14–18.
32. Efremova, M., Vento-Tormo, M., Teichmann, S.A., and Vento-Tormo, R. (2020). CellPhoneDB: inferring cell-cell communication from combined expression of multi-subunit ligand-receptor complexes. Nat. Protoc. *15*, 1484–1506.
33. Lan, R., Wu, Y., Dai, Q., and Wang, F. (2023). Gene mutations and chromosomal abnormalities in syndromes with tooth agenesis. Oral Dis. *29*, 2401–2408.
34. Liu, W., Weng, L.X., Gao, M.X., and Zhang, X.M. (2024). Applications of high performance liquid chromatography-mass spectrometry in proteomics. Se Pu *42*, 601–612.
35. Suthon, S., Perkins, R.S., Bryja, V., Miranda-Carboni, G.A., and Krum, S.A. (2021). WNT5B in Physiology and Disease. Front. Cell Dev. Biol. *9*, 667581.
36. Zhou, Y., Zheng, L., Li, F., Wan, M., Fan, Y., Zhou, X., Du, W., Pi, C., Cui, D., Zhang, B., et al. (2018). Bivalent Histone Codes on WNT5A during Odontogenic Differentiation. J. Dent. Res. *97*, 99–107.
37. Lin, M., Li, L., Liu, C., Liu, H., He, F., Yan, F., Zhang, Y., and Chen, Y. (2011). Wnt5a regulates growth, patterning, and odontoblast differentiation of developing mouse tooth. Dev. Dyn. *240*, 432–440.
38. Kaasalainen, M., Zhang, R., Vashisth, P., Birjandi, A.A., S'Ari, M., Martella, D.A., Isaacs, M., Mäkilä, E., Wang, C., Moldenhauer, E., et al. (2024). Lithiated porous silicon nanowires stimulate periodontal regeneration. Nat. Commun. *15*, 487.
39. Zhang, R., Yang, G., Wu, X., Xie, J., Yang, X., and Li, T. (2013). Disruption of Wnt/beta-catenin signaling in odontoblasts and cementoblasts arrests tooth root development in postnatal mouse teeth. Int. J. Biol. Sci. *9*, 228–236.
40. Zhang, R., Teng, Y., Zhu, L., Lin, J., Yang, X., Yang, G., and Li, T. (2015). Odontoblast beta-catenin signaling regulates fenestration of mouse Hertwig's epithelial root sheath. Sci. China Life Sci. *58*, 876–881.

41. Zhang, R., Lin, J., Liu, Y., Yang, S., He, Q., Zhu, L., Yang, X., and Yang, G. (2021). Transforming Growth Factor-beta Signaling Regulates Tooth Root Dentinogenesis by Cooperation With Wnt Signaling. Front. Cell Dev. Biol. *9*, 687099.
42. Li, W., Lin, X., Yang, H., Cao, Y., Zhang, C., and Fan, Z. (2018). Depletion of HOXA5 inhibits the osteogenic differentiation and proliferation potential of stem cells from the apical papilla. Cell Biol. Int. *42*, 45–52.
43. Chugrynina, N.M., Roginskii, V.V., Panikarovskii, V.V., Il'ina, S.B., and Antipova, Z.P. (1975). Clinical picture and morphology of Serres' glands. Stomatologiia *54*, 64–68.
44. Pagella, P., de Vargas Roditi, L., Stadlinger, B., Moor, A.E., and Mitsiadis, T.A. (2021). A single-cell atlas of human teeth. iScience *24*, 102405.
45. Gao, C., Zhang, M., and Chen, L. (2020). The Comparison of Two Single-cell Sequencing Platforms: BD Rhapsody and 10x Genomics Chromium. Curr. Genom. *21*, 602–609.
46. Angelova Volponi, A., Kawasaki, M., and Sharpe, P.T. (2013). Adult human gingival epithelial cells as a source for whole-tooth bioengineering. J. Dent. Res. *92*, 329–334.
47. Wang, S., and Qin, L. (2022). Homeostatic medicine: a strategy for exploring health and disease. Curr. Med. *1*, 16.
48. Kicheva, A., and Briscoe, J. (2023). Control of Tissue Development by Morphogens. Annu. Rev. Cell Dev. Biol. *39*, 91–121.
49. Simsek, M.F., and Özbudak, E.M. (2022). Patterning principles of morphogen gradients. Open Biol. *12*, 220224.
50. Ceriani, F., Pozzan, T., and Mammano, F. (2016). Critical role of ATP-induced ATP release for Ca2+ signaling in nonsensory cell networks of the developing cochlea. Proc. Natl. Acad. Sci. USA *113*, E7194–E7201.
51. Rodrigues, A.S., Teixeira, E.C., Antunes, L.S., Nelson-Filho, P., Cunha, A.S., Levy, S.C., de Souza Araújo, M.T., de Carvalho Ramos, A.G., Cruz, G.V., Omori, M.A., et al. (2020). Association between craniofacial morphological patterns and tooth agenesis-related genes. Prog. Orthod. *21*, 9.
52. Zhang, H., Gong, X., Xu, X., Wang, X., and Sun, Y. (2023). Tooth number abnormality: from bench to bedside. Int. J. Oral Sci. *15*, 5.
53. Wang, J., Li, G., Hu, L., Yan, F., Zhao, B., Wu, X., Zhang, C., Wang, J., Du, J., and Wang, S. (2020). Retinoic Acid Signal Negatively Regulates Osteo/Odontogenic Differentiation of Dental Pulp Stem Cells. Stem Cells Int. *2020*, 5891783.
54. Shroff, N.P., Xu, P., Kim, S., Shelton, E.R., Gross, B.J., Liu, Y., Gomez, C.O., Ye, Q., Drennon, T.Y., Hu, J.K., et al. (2024). Proliferation-driven mechanical compression induces signalling centre formation during mammalian organ development. Nat. Cell Biol. *26*, 519–529.
55. Zheng, G.X.Y., Terry, J.M., Belgrader, P., Ryvkin, P., Bent, Z.W., Wilson, R., Ziraldo, S.B., Wheeler, T.D., McDermott, G.P., Zhu, J., et al. (2017). Massively parallel digital transcriptional profiling of single cells. Nat. Commun. *8*, 14049.
56. Satija, R., Farrell, J.A., Gennert, D., Schier, A.F., and Regev, A. (2015). A. Spatial reconstruction of single-cell gene expression data. Nat. Biotechnol. *33*, 495–502.
57. McGinnis, C.S., Murrow, L.M., and Gartner, Z.J. (2019). DoubletFinder: Doublet Detection in Single-Cell RNA Sequencing Data Using Artificial Nearest Neighbors. Cell Syst. *8*, 329–337.
58. Korsunsky, I., Millard, N., Fan, J., Slowikowski, K., Zhang, F., Wei, K., Baglaenko, Y., Brenner, M., Loh, P.R., and Raychaudhuri, S. (2019). Fast, sensitive and accurate integration of single-cell data with Harmony. Nat. Methods *16*, 1289–1296.
59. Yu, G., Wang, L.G., Han, Y., and He, Q.Y. (2012). clusterProfiler: an R package for comparing biological themes among gene clusters. clusterProfiler: an R package for comparing biological themes among gene clusters OMICS *16*, 284–287.
60. Srivastava, A.K., Wang, Y., Huang, R., Skinner, C., Thompson, T., Pollard, L., Wood, T., Luo, F., Stevenson, R., Polimanti, R., et al. (2016). Human genome meeting 2016. Hum. Genom. *28*, 12.
61. Huynh-Thu, V.A., Irrthum, A., Wehenkel, L., and Geurts, P. (2010). Inferring regulatory networks from expression data using tree-based methods. PLoS One *5*, e12776.
62. Tirosh, I., Izar, B., Prakadan, S.M., Wadsworth, M.H., 2nd, Treacy, D., Trombetta, J.J., Rotem, A., Rodman, C., Lian, C., Murphy, G., et al. (2016). Dissecting the multicellular ecosystem of metastatic melanoma by single-cell RNA-seq. Science *352*, 189–196.
63. Butler, A., Hoffman, P., Smibert, P., Papalexi, E., and Satija, R. (2018). Integrating single-cell transcriptomic data across different conditions, technologies, and species. Nat. Biotechnol. *36*, 411–420.
64. Finak, G., McDavid, A., Yajima, M., Deng, J., Gersuk, V., Shalek, A.K., Slichter, C.K., Miller, H.W., McElrath, M.J., Prlic, M., et al. (2015). MAST: a flexible statistical framework for assessing transcriptional changes and characterizing heterogeneity in single-cell RNA sequencing data. Genome Biol. *16*, 278.
65. Szklarczyk, D., Gable, A.L., Lyon, D., Junge, A., Wyder, S., Huerta-Cepas, J., Simonovic, M., Doncheva, N.T., Morris, J.H., Bork, P., et al. (2019). STRING v11: protein-protein association networks with increased coverage, supporting functional discovery in genome-wide experimental datasets. Nucleic Acids Res. *47*, D607–D613.
66. Hafemeister, C., and Satija, R. (2019). Normalization and variance stabilization of single-cell RNA-seq data using regularized negative binomial regression. Genome Biol. *20*, 296.
67. Stuart, T., Butler, A., Hoffman, P., Hafemeister, C., Papalexi, E., Mauck, W.M., 3rd, Hao, Y., Stoeckius, M., Smibert, P., and Satija, R. (2019). Comprehensive Integration of Single-Cell Data. Cell *177*, 1888–1902.
68. Kall, L., Canterbury, J.D., Weston, J., Noble, W.S., and MacCoss, M.J. (2007). Semi-supervised learning for peptide identification from shotgun proteomics datasets. Nat. Methods *4*, 923–925.
69. Yang, G., Zhou, J., Teng, Y., Xie, J., Lin, J., Guo, X., Gao, Y., He, M., Yang, X., and Wang, S. (2014). Mesenchymal TGF-beta signaling orchestrates dental epithelial stem cell homeostasis through Wnt signaling. Stem Cell. *32*, 2939–2948.

STAR★METHODS

KEY RESOURCES TABLE

REAGENT or RESOURCE	SOURCE	IDENTIFIER
Antibodies		
Rabbit polyclonal Cytokeratin 6	Zenbio	Cat#R50064; RRID:AB_2721110
Rabbit polyclonal CLDN4	Zenbio	Cat#860402; RRID:AB_2721111
Rabbit polyclonal TWIST1	Zenbio	Cat#220820; RRID:AB_2721112
Rabbit polyclonal KI67	Zenbio	Cat#R50044; RRID:AB_2721113
Rabbit polyclonal FRZB	Invitrogen	Cat#PA5-104120; RRID:AB_253820758
Rabbit polyclonal ETV5	Sino Biogical	Cat#101151-T08; RRID:AB_2721114
Bacterial and virus strains		
Lentivirus	Genechem	Cat#KL100539-1
Biological samples		
Human fetal tooth	Beijing Obstetrics and Gynecology Hospital	N/A
Chemicals, peptides, and recombinant proteins		
Tissue storage solution	Biosharp	Cat#BL1167B
Phosphate-Buffered Saline	Gibco	Cat#10010023
diethyl pyrocarbonate	Invitrogen	Cat#AM9906
O.C.T. compounds	Sakura	Cat#4583
2-methylbutane	Sigma Aldrich	Cat#M32631
collagenase II	Sigma Aldrich	Cat#9001-12-1
DNase I	Sigma Aldrich	Cat#10104159001
fetal bovine serum	Gibco	Cat#A5670401
TSA-dendron-fluorophores	Perkin Elmer	Cat#NEL701A001KT
formic acid	Sigma Aldrich	Cat#28905
dispase II	Gibco	Cat#17105041
L-ascorbic acid phosphate	Sigma Aldrich	Cat#49752
BMP-3	Advanced Cell Diagnostics	N/A
SHH	Advanced Cell Diagnostics	N/A
TSA Plus Cyanine 3	Akoya	Cat#NEL744001KT
recombinant human WNT5A	R&D Systems	Cat#645-WN-010/CF
recombinant human WNT5B	R&D Systems	Cat#7347-WN-025/CF
Alizarin red S stain	Sigma Aldrich	Cat#A5533
penicillin, streptomycin	Gibco	Cat#15070063
Lipofectamine 2000	Invitrogen	Cat#11668500
Urea	Sigma Aldrich	Cat#U5378
Protease inhibitor	Sigma Aldrich	Cat#P8340
Dithiothreitol (DTT)	Sigma Aldrich	Cat#D9779
Ammonium bicarbonate buffer	Sigma Aldrich	Cat#A6141
Trypsin	Sigma Aldrich	Cat#T6567
Acetonitrile (ACN)	Sigma Aldrich	Cat#34967
Polybrene	Sigma Aldrich	Cat#TR-1003-G
Puromycin	Sigma Aldrich	Cat#P8833
DAPI	Invitrogen	Cat#D3571
4% paraformaldehyde (PFA)	Sigma Aldrich	Cat#P6148
TRIzol™ reagent	Invitrogen	Cat#15596026

(*Continued on next page*)

Continued

REAGENT or RESOURCE	SOURCE	IDENTIFIER
Reverse Transcriptase	Invitrogen	Cat#18080093
10% cetylpyridinium chloride solution	Sigma Aldrich	Cat#C5911
Protease	Advanced Cell Diagnostics	Cat#310-100
Critical commercial assays		
Single Cell 3′ GEM, Library & Gel Bead Kit V3.1	10× Genomics	Cat#1000075
Chromium Single Cell B Chip Kit	10× Genomics	Cat#1000074
Visium Spatial Gene Expression slides and Reagent Kits	10× Genomics	Cat#PN-1000184
RNAscope Multiplex Fluorescent Assay	Advanced Cell Diagnostics	Cat#323110
ALP Assay Kit	Sigma Aldrich	Cat#MAK530
Human WNT5B ELISA Kit	Zyme Chain Biotechnology	Cat#EH1815
H&E kit	Vector Laboratories	Cat#H-3401
QuantiTect SYBR Green PCR Kit	Qiagen	Cat#204143
Deposited data		
scRNA-seq data	This paper	CNP0006291
ST data	This paper	CNP0006291
secretome data	This paper	CNP0006291
Experimental models: Cell lines		
HEK293T	China Cell Bank	Cat#SCC-293T
Experimental models: Organisms/strains		
NU/NU mice	Charles River	Cat#403
Software and algorithms		
Cell Ranger Single Cell Software Suite v6.1.2	Zheng et al.[55]	https://www.10xgenomics.com/support/software/cell-ranger/latest
Seurat v4.1.1	Satija et al.[56]	https://github.com/satijalab/seurat/releases/tag/v4.1.1
DoubletFinder v2.0.3	McGinnis et al.[57]	https://github.com/chris-mcginnis-ucsf/DoubletFinder/releases/tag/v2.0.3
Harmony v0.1.0	Korsunsky et al.[58]	https://github.com/immunogenomics/harmony
ClusterProfiler	Wu et al.[59]	https://bioconductor.org/packages/release/bioc/html/clusterProfiler.html
SCENIC v1.1.2	Van de Sande et al.[60]	https://github.com/aertslab/SCENIC
GENIE3	Huynh-Thu et al.[61]	https://github.com/GENIE3/GENIE3
CellPhoneDB v4.0.0	Efremova et al.[32]	https://github.com/Teichlab/CellPhoneDB
Monocle 3	Cao et al.[22]	https://github.com/cole-trapnell-lab/monocle3
Velocyto (Python-based)	La Manno et al.[21]	https://github.com/velocyto-team/velocyto.py
SeuratWrappers v0.1.0	Tirosh et al.[62]	https://github.com/Teichlab/SeuratWrappers
Space Ranger toolkit		https://support.10xgenomics.com/spatial-gene-expression/software/overview/welcome
Jackstraw	Butler et al.[63]	https://github.com/satijalab/seurat
MAST	Finak et al.[64]	https://github.com/RGLab/MAST
GeneSwitches	Cao et al.[29]	https://github.com/gmarkow/GeneSwitches
Proteome Discoverer v2.4		https://www.thermofisher.cn/cn/zh/home/industrial/mass-spectrometry/liquid-chromatography-mass-spectrometry-lc-ms/lc-ms-software/multi-omics-data-analysis/proteome-discoverer-software.html
STRING-db	Damian et al.[65]	
SCTransform	Hafemeister et al.[66]	https://github.com/satijalab/seurat

(*Continued on next page*)

Continued

REAGENT or RESOURCE	SOURCE	IDENTIFIER
TransferData	Tim et al.[67]	https://github.com/satijalab/seurat
Percolator	Lukas et al.[68]	https://github.com/percolator/percolator
Other		
Transwell plates	Corning	Cat#3460

EXPERIMENTAL MODEL AND STUDY PARTICIPANT DETAILS

Human fetal tooth tissue

Twelve human developmental tooth tissues were included in the study. Post-conceptional and clinical age were determined through clinical ultrasound and stage-dependent anatomical landmarks of the embryos at 9–10, 12, 15, and 22 PCW. Samples were obtained from elective surgical abortions at the Beijing Obstetrics and Gynecology Hospital (BOGH), Capital Medical University (CMU), with written informed consent from the pregnant individuals. All participants were Chinese-speaking and above 18 years old. The midwives and gynecologists involved in patient care did not partake in the research. Tooth tissues were dissected in a tissue storage solution (Biosharp, BL1167B) on ice, and then transferred immediately to the Beijing Laboratory of Oral Health (BLOH) for further processing. Gender information of the tooth tissues was computationally derived. Specifically, tooth buds at 9–10 and 12 PCW were male, while the tooth buds at 15 and 22 PCW were female. Tooth germs of incisors and molars were dissected in Phosphate-Buffered Saline (PBS) (Gibco, 10010023) treated with diethyl pyrocarbonate (DEPC) (Invitrogen, AM9906) on ice. Unnecessary soft tissues near the mandible were cut to expose all five tooth germs (two incisors, one canine, and two molars) on each side to ensure accuracy for scRNA-seq of tooth sampling and to avoid tissue contamination for ST. Tooth buds at 9–10, 12, and 15 PCW were subjected to ST and scRNA-seq analyses, while those at 12, 15, and 22 PCW underwent IF analysis. Additionally, tooth buds at 12 PCW were utilized for secretome and tissue recombination studies. In order to have comprehensive cell types, biological replicates ($n = 2$, one incisor and one molar) were provided at each gestational age for both scRNA-seq and ST. The collected tooth buds were washed in cold PBS and then proceeded directly to digestion. The dissected mandibles were embedded in cold O.C.T. compounds (Sakura, 4583) by submersion in isopentane (Sigma Aldrich, 4583) pre-cooled to 80°C in dry ice for ST; they were then fixed in 4% paraformaldehyde (PFA) (Sigma Aldrich, P6148) at 4°C overnight. The present study is approved by the Ethics Commission of Beijing Friendship Hospital, CMU (2021-P2-198-02); the BLOH, CMU (Z2022SY064); the BOGH, CMU (2023-KY-082-01). All experiments were performed in accordance with relevant guidelines and regulations.

Establishment of human primary DE and DM cells

Human primary DE cells and DM cells were prepared from tooth germs of 11–12 PCW. The isolated tooth germs were incubated in 1.2 U/ml dispase II (Gibco, 17105041) and 20 U/ml DNase I (Gibco, 10104159001) for 10.5 min at room temperature. The epithelial tissues were separated from the mesenchymal tissues using a fine needle. The DE were surgically minced and plated on dishes in keratinocyte SFM (1×), without calcium chloride (Gibco, A15170-01), supplemented with 15% (fetal bovine serum (FBS) (Gibco, A5670401). The mesenchymal parts were removed from the DE and minced into small pieces, followed by digestion with 3 mg/mL collagenase type I (Sigma Aldrich, C0130) and 4 mg/mL dispase II for 1 h at 37°C. The cells were expanded with α-MEM culture medium (Gibco, 12561072), supplemented with 15% FBS, 100 units/ml penicillin, 100 mg/mL streptomycin, and 25 μg/mL Amphotericin B (Gibco, 15070063), and incubated at 37°C in 5% CO_2.

METHOD DETAILS

Droplet based scRNA-seq

Cell capture and complementary DNA (cDNA) synthesis were performed using the Single Cell 3′ GEM, Library & Gel Bead Kit V3.1 (10× Genomics, 1000075) and Chromium Single Cell B Chip Kit (10× Genomics, 1000074). The cell suspension (300–600 living cells per microliter, determined by Count Star) was loaded onto the Chromium single cell controller (10× Genomics, 1000073) to generate single-cell gel beads in the emulsion, following the manufacturer's protocol. In short, single cells were suspended in PBS containing 0.04% bovine serum albumin. Approximately 6,000 cells were added to each channel, while approximately 3,000 cells were recovered as target cells and then amplified. Quality assessment was conducted using an Agilent 2400 (performed by CapitalBio Technology, Beijing). According to the manufacturer's instructions, scRNA-seq libraries were constructed using the Single Cell 3′ Library and Gel Bead Kit V3.1. The libraries were finally sequenced using an Illumina Novaseq 6000 sequencer with a sequencing depth of at least 100,000 reads per cell, using a pair-end 150 bp (PE150) reading strategy (performed by CapitalBio Technology, Beijing).

Spatial transcriptomics

Cryosections were cut at a thickness of 10 μm and mounted onto the GEX arrays. The sections were placed on a Thermocycler Adaptor with the active surface facing up and incubated for 1 min at 37°C. They were then fixed for 30 min with methyl alcohol at −20°C and stained with haematoxylin and eosin (H&E) (Eosin Dako). Brightfield images were taken using a Leica DMI8 whole-slide scanner at a resolution of 10×.

Visium Spatial Gene Expression was processed using Visium Spatial Gene Expression slides and Reagent Kits (10× Genomics, PN-1000184). For each well, a Slide Cassette was used to create leakproof wells for adding reagents. 70 μL of permeabilization enzyme was added and incubated at 37°C for 36 min. Each well was then washed with 100 μL of SSC, and 75 μL of reverse transcription Master Mix was added for cDNA synthesis.

At the end of the first-strand synthesis, the RT Master Mix was removed from the wells. Add 75 μL of 0.08 M KOH and incubate for 5 min at room temperature. Then, remove the KOH from the wells and wash with 100 μL of EB buffer. Add 75 μL of the Second Strand Mix to each well for the second-strand synthesis. cDNA amplification was performed on a S1000TM Touch Thermal Cycler (Bio-Rad).

According to the manufacturer's introduction, Visum spatial libraries were constructed using the Visum Spatial Library Construction Kit (10× Genomics, PN-1000184). The libraries were finally sequenced using an Illumina NovaSeq6000 sequencer with a sequencing depth of at least 100,000 reads per spot and a PE150 reading strategy (performed by CapitalBio Technology, Beijing).

Primary analysis of raw read data

The raw scRNA-seq data were pre-processed (demultiplexing cellular barcodes, read alignment to the human reference genome build, and generation of a gene count matrix) using the Cell Ranger Single Cell Software Suite (v6.1.2)[55] provided by 10× Genomics. Detailed QC metrics were generated and evaluated. Cells with low complexity libraries or likely cellular debris (in which detected transcripts are aligned to fewer than 200 genes) were filtered out and excluded from subsequent analyses. A total of 45,512 cells were identified.

Quality control, dimension reduction and clustering

Barcodes with fewer than 500 unique genes, fewer than 1,000 UMI counts, and more than 15% of transcript counts derived from mitochondrially encoded genes were discarded. We used functions from Seurat v4.1.1[56] for dimension reduction and clustering. The data was normalized and scaled using the SCTransform[66] function. To identify major axes of variation within our data, we first examined only highly variable genes across all cells, yielding approximately 2,000 variable genes. An approximate principal component (PC) analysis was applied to the cells to generate 100 PCs. Using a combination of the Jackstraw function[63] in Seurat and observing the "elbow" of the standard deviations of PCs, we chose the top 50 PCs for subsequent clustering and visualization. Doublets were detected, marked, and removed for each sample with DoubletFinder v2.0.3.[57]

The batch effect between the six samples was removed using Harmony v0.1.0.[58] To identify clusters of transcriptionally similar cells, we employed unsupervised clustering as described above, using the FindClusters tool within the Seurat R package with default parameters and a resolution of 1.2. Finally, the UMAP algorithm was applied to visualize cells in a two-dimensional space.

Differentially expressed genes analysis

To identify differentially expressed genes (DEGs), we used the Seurat FindMarkers function based on Model-based Analysis of Single-cell Transcriptomics (MAST)[64] with default parameters. We selected genes with a Bonferroni-adjusted *pp-value* cutoff of less than 0.05 and an average log (Fold Change) value greater than 0.25 as DEGs. Similarly, the FindMarkers function was used to identify signature genes by comparing cluster pairs of interest. GO (Gene Ontology) and KEGG (Kyoto Encyclopedia of Genes and Genomes) enrichment analyses of significant genes were performed using the R package ClusterProfiler.[59]

Cell type annotation

The cell type identity of each cluster was determined by the expression of canonical markers found in the DEGs, tooth canonical marker genes, the published literature. Key cell population markers were validated using IF staining. Dot plots and violin plots displaying the expression of markers used to identify each cell type were generated using the Seurat V4.1.1 DotPlot/Vlnplot function. Finally, eight cell types were carefully annotated.

Subcluster analysis

Subcluster analysis was performed to investigate the heterogeneity within the DE, DP and DF populations.

Trajectory analysis

We used Monocle 3 to generate the pseudotime trajectory across the DE and DP cells. The cells were input into Monocle 3 to infer cluster and lineage relationships within a given cell type. UMAP embeddings and cell subclusters generated from Seurat were converted to a cell dataset object using SeuratWrappers (v.0.1.0).[22] Trajectory graph learning and pseudotime measurement were performed through reversed graph embedding.

GeneSwitches analysis

Following monocle trajectory analysis, pseudo-times were subsetted using choose_graph_segments (cds, reduction_method = "UMAP", starting_pr_node = NULL, return_list = FALSE, clear_cds = TRUE). Expression plots were generated using plot_cells. Analysis of gene switching on and off in pseudo-time was performed using the GeneSwitches package.

Velocity analysis

The Python-based Velocyto command-line tool and Velocyto R package[21] were used as instructed for RNA velocity analysis. Velocyto calculated the single-cell trajectory/directionality using spliced and unspliced reads. From the loom files generated by the command-line tool, we extracted the DE and DP cells in R to perform Velocity analysis using the SeuratWrappers package.[62] RNA velocity was estimated using a gene-relative model with kNN cell pooling (k = 25). RNA velocity was visualized on the UMAP embedding with the parameter n = 200. scVelo was used to perform Velocity analysis of integrative datasets combining different stages.

Gene regulatory network inference

To gain a better understanding of the transcription factors that activate gene expression in DE and DP cells, we utilized the R package SCENIC.[60] This computational method detects gene regulatory networks and was used to analyze network activity in dental mesenchymal cells in order to identify recurrent cellular states. Transcription factors were identified using[32,61] and compiled into regulons, which were then subjected to *cis*-regulatory motif analysis. The activity of these regulons was then scored using AUCell.

Cellular interaction analysis

Cellular interactions between cell types were computed based on ligand-receptor co-expression using the CellPhoneDB (v4.0.0) tool[32] with default settings and log-transformed SCTransform normalized counts as input. The analysis of interactions between DE and DP (9–10 PCW), enamel knot/inner enamel epithelium, and coronal dental papilla cells (12 and 15 PCW) was conducted for each individually. Only cell types with more than 20 cells per patient were included. To calculate the average number of interactions, we summed all significant (*pp-value* <0.05) interactions between two cell types per sample/donor and averaged this number over samples/donors. To calculate the interaction strength between two cell types across patients, we summed up the mean expression of all ligand and receptor pairs as calculated by CellPhoneDB across all samples.

Process and quality control of spatial RNA-seq

The raw sequencing reads of spatial RNA-seq were aligned to the GRCh38 human reference genome using the Space Ranger toolkit (v4.0.0) from 10× Genomics. The SCTransform function of Seurat was used to normalize and scale gene expression, as well as to regress out the effect of mitochondrial gene expression percentage. The TransferData[67] function of Seurat was then performed to combine cluster information from scRNA-seq data with spatial information from spatial RNA-seq data. Corresponding clusters for each spot were predicted using scRNA-seq data as the anchor set, and each spot was marked with the corresponding cluster with the highest score.

The identification and quantitation of protein

All RAW files were analyzed using the Proteome Discoverer suite (Thermo Fisher Scientific, v2.4). MS2 spectra were searched against the UniProt Homo sapiens SP proteome database (20,361 target sequences downloaded on 2022-03-17). The Sequest HT search engine was used, and parameters were specified as follows: fully tryptic specificity, a maximum of two missed cleavages, a minimum peptide length of 6, fixed carbamidomethylation of cysteine residues (+57.02146 Da), variable modifications for oxidation of methionine residues (+15.99492 Da), a precursor mass tolerance of 15 ppm, and a fragment mass tolerance of 0.02 Da for MS2 spectra collected in the Orbitrap. Percolator[68] was used to filter peptide spectral matches and peptides to a false discovery rate of less than 1%. After spectral assignment, peptides were assembled into proteins and further filtered based on the combined probabilities of their constituent peptides to a final FDR of 1%. By default, the top matching protein, or 'master protein', is the protein with the largest number of unique peptides and the smallest value in percent peptide coverage (that is, the longest protein). Only unique and razor (that is, parsimonious) peptides were considered for quantification.

The functional analysis of protein

GO and InterPro analyses were conducted using the InterProScan-5 program against the non-redundant protein database. The Clusters of Orthologous Groups and KEGG databases were used to analyze the protein families and pathways. The probable interacting partners were predicted using the STRING-db server[65] (http://string.embl.de/) based on related species. STRING is a database of both known and predicted protein-protein interactions. The enrichment pipeline was used to perform enrichment analyses of GO and KEGG, respectively.

I, RNAscope *in situ* hybridization (ISH) and H&E staining

The paraffin-embedded tissue blocks were cut at a thickness of 5 μm onto slides. The slides were then deparaffinized by passing through an ethanol gradient and heat-induced epitope retrieval was performed at 96°C for 25 min in pH 6.0 citrate buffer (Amresco, ZLI-9064). Peroxidase was blocked, and species-specific primary antibodies were then added and incubated overnight at 4°C.

Primary antibodies used Cytokeratin 6 (Zenbio, R50064,1:400 dilutions), CLDN4 (Zenbio, 860402, 1:200 dilutions), TWIST1 (Zenbio, 220820, 1:200 dilutions), KI67 (Zenbio, R50044, 1:200 dilutions), FRZB (Invitrogen, PA5-104120, 1:200 dilutions), ETV5 (Sino Biogical, 101151-T08, 1:2500 dilutions). This was followed by the addition of species-specific secondary antibodies. The stain was developed with TSA-dendron-fluorophores (PerkinElmer, NEL701A001KT) according to the manufacturer's instructions. Cells were then counterstained with DAPI (Invitrogen, D3571).

ISH was performed using an RNAscope Multiplex Fluorescent Assay (Advanced Cell Diagnostics, 320850). Briefly, tissues were fixed in 4% PFA overnight at room temperature before cryosectioning to 6 μm thickness. Target retrieval was performed on the sections for 5 min at 95°C–100°C, followed by protease (Advanced Cell Diagnostics, 310-100) treatment for 7 min at 40°C. Probes for *BMP-3*, *SHH*, *FGF3* (Advanced Cell Diagnostics) were then hybridized for 2 h at 40°C, followed by RNAscope amplification reagents provided in the RNAscope Multiplex Fluorescent Reagent Kit. The signal was detected using TSA Plus Cyanine 3 (PerkinElmer, NEL751A). Cells were then counterstained with DAPI.

H&E staining was carried out by deparaffinization in a similar manner, followed by the addition of stains as described in the H&E kit (Vector Laboratories, H-3401).

Collection of the supernatant, protein extraction, digestion and desalination

Cultured primary human DE and DM cells at passage 0 were used for secretome collection. 300 μL of 8 M urea (Sigma Aldrich, U5378) was added to the sample and the protease inhibitor (Sigma Aldrich, P8340) was added at a 10% concentration of the lysate. After centrifuging at 14,100×g for 20 min, the supernatant was collected. The protein concentration was determined using the Bradford method, and the remaining sample was frozen at −80°C.

A 100 μg aliquot of extracted proteins from each sample was then subjected to reduction by adding a 200 mM dithiothreitol solution (Sigma Aldrich, D9779) and incubating at 37°C for 1 h. The sample was then diluted 4 times by adding 25 mM ammonium bicarbonate buffer (Sigma Aldrich, A6141). Next, trypsin (Sigma Aldrich, T6567) was added at a ratio of 1:50 (trypsin: protein) and the sample was incubated at 37°C overnight.

The next day, 50 μL of 0.1% formic acid (FA) (Sigma Aldrich, 339251) was added to terminate the digestion. 100 μL of 100% acetonitrile (ACN) (Sigma Aldrich, 34967) was used to wash the C18 column, and then centrifuged at 1200 rpm for 3 min. The columns were washed once with 100 μL of 0.1% FA and centrifuged at 1200 rpm for 3 min. The EP tubes were replaced and centrifuged at 1200 rpm for 3 min. The columns were then washed twice with 100 μL of 0.1% FA and centrifuged at 1200 rpm for 3 min. Next, 100 μL of water (pH = 10) was added for one final wash. The EP tubes were replaced and the samples were eluted with 70% ACN. The eluents from each sample were combined and then lyophilized. They were stored at −80°C until loading.

Liquid chromatography (LC)-mass spectrometer (MS)/MS analysis

Nanoflow LC-MS/MS analysis of tryptic peptides was conducted on a quadrupole Orbitrap mass spectrometer (Thermo Fisher Scientific) coupled to an EASY nLC 1200 ultra-high-pressure system (Thermo Fisher Scientific) via a nano-electrospray ion source. 500 ng of peptides were loaded onto a 25 cm column (150 μm inner diameter, packed using ReproSil-Pur C18 AQ 1.9 μm silica beads; Beijing Qinglian Biotech). Peptides were separated using a gradient from 8% to 12% solvent B (80% ACN +0.1% formic acid in water) in 5 min, then 12%–30% solvent B in 33 min and stepped up to 40% in 7 min followed by a 15-min wash at 95% solvent B at 600 nL per minute. The total duration of the run was 60 min. The column temperature was kept at 60°C using an in-house-developed oven. Briefly, the mass spectrometer was operated in "top-40" data-dependent mode, collecting MS spectra in the Orbitrap mass analyzer (120,000 resolution, 350–1500 m/z range) with an automatic gain control (AGC) target of 3E6 and a maximum ion injection time of 80 ms. The most intense ions from the full scan were isolated with an isolation width of 1.6 m/z. Following higher-energy collisional dissociation (HCD) with a normalized collision energy (NCE) of 27, MS/MS spectra were collected in the Orbitrap (15,000 resolution) with an AGC target of 5E4 and a maximum ion injection time of 45 min. Precursor dynamic exclusion was enabled with a duration of 16 s.

Plasmid construction and lentivirus production

The lentiviral vector expressing short guide RNA (sgRNA) targeting the sequence of the WNT5B gene (5′-TTCTGACAGACGC CAACTCCT-3′) and a negative control sgRNA (5′-CGCTTCCGCGGCCCGTTCAA-3') was synthesized and cloned into a GV392 vector under the control of a K14 promoter (Genechem). The recombinant plasmid was verified by DNA sequencing to confirm correct insertion of the sgRNA sequences. The lentiviral particles were produced by co-transfecting the recombinant vector into HEK293T cells (China Cell Bank, SCC-293T) using Lipofectamine 2000 (Invitrogen, 11668500) along with two helper plasmids, psPAX2 and pMD2.G, according to the manufacturer's instructions. The supernatant containing lentiviral particles was collected 72 h post-transfection, centrifuged at 3000×g for 10 min at 4°C to remove cell debris, and filtered through 0.45 μm cellulose acetate filters. The virus titer was determined by fluorescence-activated cell sorting (FACS) analysis of GFP-positive human primary DE cells, yielding approximately 1 × 10^8 transducing units (TU)/mL. The purified lentiviral stocks were aliquoted and stored at −80°C until further use.

In vitro treatment assay

Cultured primary human DM cells at passage 3 or 4 were used for *in vitro* experiments. On the first day of differentiation (designated as Day 0), the human DM cells were treated with recombinant human WNT5B (rhWNT5B) (R&D Systems, 7347-WN-025/CF) at

concentrations of 100 ng/mL. The media were used as described previously and changed every 2–3 days. Samples were collected on days 3, 7, and 14 for subsequential analysis (Figure 5J). To test the virus infection efficiency, primary human DE cells at passage 0 were seeded at 1×10^5 cells per well in 12-well plates and maintained in the previously described epithelium culture medium, with medium changes every 2–3 days, until reaching approximately 20–30% confluence. To specifically knock down WNT5B, two experimental groups were established: DE-K14-iWnt5B-LV (lentivirus carrying shRNA targeting WNT5B) and DE-K14-NC-LV (negative control lentivirus). The multiplicity of infection (MOI) was set to 50 based on preliminary experiments. Lentiviral particles (1×10^8 TU/ml) were mixed with complete medium containing 5 μg/mL polybrene (Sigma Aldrich, TR-1003-G) and added to the cells. After a 16-h incubation at 37°C, the viral supernatant was replaced with fresh medium, and the cells were cultured for another 72 h. Antibiotic selection was then initiated by adding 1 μg/mL puromycin (Sigma Aldrich, P8833) to the culture, with the selection medium replaced every 1–2 days for a total of 6 days until surviving cells had recovered and proliferated. At this time, the efficiency of lentiviral infection was evaluated by fluorescence microscopy (magnification, ×10) for both the DE-K14-iWnt5B-LV and DE-K14-NC-LV groups. After selection, hDEs were maintained in the lower chambers of a Transwell plate equipped with a 0.4 μm pore-size membrane (Corning, 3460). Human DM cells at passages 3–4 were seeded in the upper chamber at a density of 2.5×10^4 cells per well and co-cultured with the transduced hDEs for 7 days. During the co-culture period, the medium was changed every 2–3 days. hDE and hDM cells were harvested on days 3, 5, and 7 for quantitative reverse transcription PCR (RT-qPCR) analysis, and hDE supernatants were collected for enzyme linked immunosorbent assay (ELISA). To compare the stimulatory differentiation capacities between WNT5A and WNT5B, passage 3–4 hDM cells were seeded at 1×10^5 cells per well in 12-well plates using differentiation medium (Procell, PD-014) supplemented with either rhWNT5A (R&D Systems, 645-WN-010/CF) or rhWNT5B at 10 ng/mL or 100 ng/mL. The medium was changed every 2–3 days. On Day 7, cells were collected for RT-qPCR analysis, while on Days 7 and 14, ALP staining and Alizarin Red staining were performed, respectively, to assess odontogenic differentiation.

ALP staining

After 7 days of induction, the cells were fixed in 4% PFA, washed with PBS, and stained with an ALP Assay Kit (Sigma Aldrich, MAK530) to assess odontogenic differentiation. The intensity of ALP staining was visually inspected to evaluate the differentiation status.

Alizarin red S staining

After 14 days of differentiation induction, cells were fixed and stained with a 2% Alizarin Red S solution (Sigma Aldrich, A5533) to detect calcium deposits. Semi-quantitative analysis of mineralized nodules was performed by dissolving the dye in a 10% cetylpyridinium chloride solution (Sigma Aldrich, C5911) and measuring the absorbance at 562 nm.

RT-qPCR

The RNA was extracted from the collected samples using TRIzol reagent (Invitrogen, 15596026) according to the manufacturer's instructions. The extracted RNA was reverse transcribed into cDNA using oligo (dT) primers and Reverse Transcriptase (Invitrogen, 18080093). RT-qPCR was performed using a QuantiTect SYBR Green PCR Kit (Qiagen, 204143) on an iCycler iQ Multi-Color Real-Time PCR Detection System (Bio-Rad, 170–8740). *GAPDH* was used as an internal control to normalize the expression of target genes. Relative expression levels of the target genes were calculated using the ΔΔCt method.

The primers used for RT-qPCR were as follows:

GAPDH:
Forward: 5′-GCACCGTCAAGGCTGAGAAC-3′
Reverse: 5′-ATGGTGGTGAAGACGCCAGT-3′
ALP:
Forward: 5′-AACATCAGGGACATTGACGTG-3′
Reverse: 5′-GTATCTCGGTTTGAAGCTCTTCC-3′
DMP-1:
Forward: 5′-GCAGAGTGATGACCCAGAG-3′
Reverse: 5′-GCTCGCTTCTGTCATCTTCC-3′
DSPP:
Forward: 5′-GGGATGTTGGCGATGCA-3′
Reverse: 5′-CCAGCTACTTGAGGTCCATCTTC-3′
WNT5B:
Forward: 5′-TTCTGACAGACGCCAACTC-3′
Reverse: 5′-TGACTCTCCCAAAGACAGATG-3'.

ELISA

The supernatants of hDEs in the co-culture system were harvested on days 3, 5, and 7. The WNT5B concentrations in the supernatants of the WNT5B knockdown group and the control group were determined using the Human WNT5B ELISA Kit (Zyme Chain Biotechnology, EH1815). The kit was operated according to the product data sheet.

Tissue recombination and subrenal culture

Human DE from the cap stage and lip mesenchyme from the same embryo at 11–12 PCW was isolated and recombined. All recombinants were further cultured in the Trowell-type organ culture system which have been reported previously[69] for 18 h prior to being subjected to subrenal culture in adult NU/NU mice (Charles River, 403). All animal studies were conducted in accordance with the official ethical guidelines and protocols approved by the Ethics Committee of Capital Medical University (AEEI-2023-087). Grafts were harvested after 3 months in subrenal culture and then processed for histological analyses.

QUANTIFICATION AND STATISTICAL ANALYSIS

Data were analyzed using GraphPad Prism (v8.0). For comparisons between two groups, unpaired t-tests were performed, with significance set at $p < 0.05$. For comparisons among multiple groups, one-way ANOVA followed by Tukey's post hoc test was used. All experiments were performed in triplicates, and results are presented as means ± standard deviation (SD) from at least three independent experiments. Statistical significance was determined with $p < 0.05$, $p < 0.01$, and $p < 0.001$ indicated in the figures with the *, **, and *** symbols, respectively (Figures 5J and 5K, and 5L).